Catalytic Hydrogenation of Renewable Levulinic Acid to γ-Valerolactone

Genuino, Homer C.; Van De Bovenkamp, Henk H.; Wilbers, Erwin; Winkelman, Jozef G.M.; Goryachev, Andrey; Hofmann, Jan P.; Hensen, Emiel J.M.; Weckhuysen, Bert M.; Bruijnincx, Pieter C.A.; Heeres, Hero J.

Published in:
ACS Sustainable Chemistry and Engineering

DOI:
10.1021/acssuschemeng.9b07678

ACS Sustainable Chemistry & Engineering

pubs.acs.org/journal/ascecg

Research Article

Catalytic Hydrogenation of Renewable Levulinic Acid to γ-Valerolactone: Insights into the Influence of Feed Impurities on Catalyst Performance in Batch and Flow Reactors

Homer C. Genuino, Henk H. van de Bovenkamp, Erwin Wilbers, Jozef G. M. Winkelman, Andrey Goryachev, Jan P. Hofmann, Emiel J. M. Hensen, Bert M. Weckhuysen,* Pieter C. A. Bruijnincx,* and Hero J. Heeres*

Cite This: ACS Sustainable Chem. Eng. 2020, 8, 5903−5919

Read Online

ACCESS | Metrics & More | Article Recommendations | Supporting Information

ABSTRACT: γ-Valerolactone (GVL) is readily obtained by the hydrogenation of levulinic acid (LA) and is considered a sustainable platform chemical for the production of biobased chemicals. Herein, the performance and stability of Ru-based catalysts (1 wt % Ru) supported on TiO_2 (P25) and ZrO_2 (monoclinic) for LA hydrogenation to GVL is investigated in the liquid phase in batch and continuous-flow reactors using water and dioxane as solvents. Particular attention is paid to the influence of possible impurities in the LA feed on catalyst performance for LA hydrogenation. Benchmark continuous-flow experiments at extended times on-stream showed that the deactivation profiles are distinctly different for both solvents. In dioxane, the Ru/ZrO_2 catalyst is clearly more stable than Ru/TiO_2, whereas the latter is slightly more stable in water. Detailed characterization studies on spent catalysts after long run times showed that the deactivation of Ru/TiO_2 is strongly linked to the reduction of a significant amount of Ti^{4+} species of the support to Ti^{3+} and a decrease in the specific surface area of the support in comparison to the fresh catalyst. Ru/ZrO_2 showed no signs of support reduction and displayed morphological and structural stability; however, some deposition of carbonaceous material is observed. Impurities in the LA feed such as HCOOH, H_2SO_4, furfural (FFR), 5-hydroxymethylfurfural (HMF), humins, and sulfur-containing amino acids impacted the catalyst performance differently. The results reveal a rapid yet reversible loss of activity for both catalysts upon HCOOH addition to LA, attributed to its preferential adsorption on Ru sites and possible CO poisoning. A more gradual drop in activity is found when cofeeding HMF, FFR, and humins for both solvents. The presence of H_2SO_4, cysteine, and methionine all resulted in the irreversible deactivation of the Ru catalysts. The results obtained provide new insights into the (ir)reversible (in)sensitivity of Ru-based hydrogenation catalysts to potential impurities in LA feeds, which is essential knowledge for next-generation catalyst development.

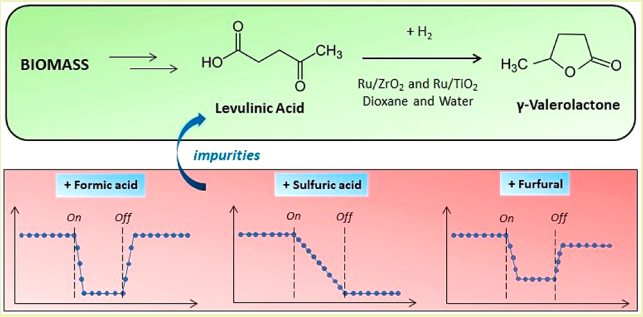

KEYWORDS: *Biobased chemicals, Catalyst stability, Catalyst deactivation, Ruthenium catalysts, Zirconia and titania supports*

INTRODUCTION

Levulinic acid (LA) is a promising, renewable starting material for the production of a variety of biobased compounds such as γ-valerolactone (GVL) and the corresponding esters.[1−5] GVL in particular has attracted considerable attention due to its potential use as a green solvent and a sustainable liquid fuel additive and for the synthesis of polymer precursors like adipic acid and diols.[6−9] A wide range of supported mono- and bimetallic catalysts have been developed to obtain high GVL yields from LA, with Ru-based catalysts typically performing the best.[10,11] From a green chemistry perspective, the reaction is of high interest because it uses a catalyst and a biobased feed (LA), it is best performed in water (an environmentally benign solvent), and it can use green hydrogen (e.g., from water electrolysis and renewable electricity). While the majority of the rapidly expanding literature for this conversion reports on the development of active and selective catalysts, catalyst stability, especially in the liquid phase, is far less investigated.[11−15] Recently, we reported on the activity, selectivity, and stability of Ru-based catalysts supported on ZrO_2 (monoclinic), TiO_2 (P25), and activated carbon (C) for this conversion in dioxane.[16] The latter is a common organic solvent used for LA hydrogenation to mimic conversions in

Received: December 24, 2019
Revised: March 7, 2020
Published: March 25, 2020

neat GVL for practical reasons of costs and analysis. All catalysts initially showed high GVL yields in a batch setup; however, large differences in catalyst stability were observed using batch recycle studies. Ru/ZrO_2 outperformed both the Ru/C and Ru/TiO_2 benchmark catalysts, displaying high activity, selectivity, and stability upon repetitive recycling.[16] For the latter, the deactivation was attributed to a reduction of the TiO_2 support and a detrimental strong substrate-induced metal−support interaction resulting in partial coverage of Ru.[15,16] In addition to work in dioxane, a large number of solvents has been screened, with water typically showing the best results in terms of catalyst performance.[17,18] The use of water leads to superior reaction rates compared to organic solvents without compromising the selectivity to GVL. Typically, reaction rates at 90 °C for Ru-based catalysts are comparable to those in dioxane at 150 °C.[11,19−23]

Catalyst deactivation by feed impurities is another important yet somewhat overlooked challenge for the efficient valorization of biomass. In an industrial process, for example, biogenic compounds (e.g., proteins) or process-derived chemicals (byproducts, reagents, or catalysts) can be carried over from preceding biorefining- or biomass-upgrading processes and potentially poison catalysts used downstream. The influence of such impurities will greatly depend on the nature of the catalyst (i.e., type of metal, particle size, and support effects), reactor configuration, process parameters (i.e., concentration, solvent, reactive atmosphere, pressure, temperature, etc.) under which the catalysts will be employed.

Several systematic studies on the detrimental effects of impurities on the performance of Ru catalysts used for the hydrogenation of biomass-derived components have been reported. For instance, Arena reported on the deactivation of a Ru/Al_2O_3 catalyst during the hydrogenation of glucose to sorbitol by sulfur from sodium sulfite, Fe from the reactor wall, and gluconic acid formed *in situ* from the oxidation of glucose with dissolved oxygen.[24] Elliott et al. extended this work to the hydrogenation of glucose and xylose in a stirred batch reactor using Ru/TiO_2 (rutile) and reported severe catalyst deactivation by amino acids and cations such as NH_4^+ and Ca^{2+}.[25] Protein fragments in biomass feedstocks can also severely interfere with the Ru-based catalysts.[25−28] For example, Zhang et al. reported on a substantial loss of activity in the Ru/C-catalyzed hydrogenation of actual fermentation-derived lactic acid.[26] Irreversible catalyst deactivation was attributed to pore plugging by proteins (i.e., albumin) and strong adsorption of sulfur-containing amino acids such as cysteine and methionine to the active metal sites.[26] A more recent study by Wang et al. showed that sulfur-containing species in bio-oil poison a Ru/TiO_2 catalyst used for hydrogenation of various components of bio-oils.[29] Catalyst regeneration by calcination to remove these contaminants is difficult, as the high temperatures used for calcination can lead to undesirable transformations of the active phase and the support.

In addition to external impurities, byproducts and reagents from earlier processing steps may also affect catalyst performance. The production of LA, for example, will typically involve the use of (mineral) acids. When not completely removed upon work up, such acid impurities and their salts (after neutralization) are expected to affect catalyst performance for downstream LA hydrogenation to GVL. For example, Braden et al. demonstrated that an H_2SO_4 impurity had a detrimental effect on the activity of a Ru/C catalyst in the LA hydrogenation in water, whereas a RuRe/C bimetallic Ru-on-carbon catalyst was less active but more stable in the presence of the same impurity.[30] Recently, we found that ZrO_2-supported Ru catalysts, again in strong contrast to the benchmark Ru/C catalyst as well as RuRe/C and RuMo/C bimetallic catalysts, remained active in LA hydrogenation in dioxane in the presence of H_2SO_4 when performed in a batch setup.[31] This remarkable stability of Ru/ZrO_2 against H_2SO_4 deactivation was attributed to the sulfate ion adsorption capacity of the oxide-based support, which thus essentially acts as a scavenger.[31]

In addition to sulfuric acid, byproducts from LA synthesis, such as sugar derivatives like 5-hydroxymethylfurfural (HMF) and furfural (FFR), are potentially present in the feed, as well as coproduced formic acid (HCOOH). HMF and FFR are known to adsorb on Ru sites and as such may reduce the activity for LA hydrogenation. For instance, Dwiatmoko et al. demonstrated that the presence of FFR and HMF negatively affected the activity of a Ru/C-catalyst for the hydrodeoxygenation of lignin-derived phenolic compounds.[32] Combined experimental and density functional theory calculations on a Ru(0001) surface showed that (HMF) and furfural (FFR) inhibited the rate of hydrogenation of guaiacol by competitive adsorption at the active Ru sites.[32]

In addition, some of the sugar-based compounds can undergo side reactions (e.g., polymerization) that result in the formation of high molecular weight humins and their precursors, which might cause fouling of a catalyst surface by deposition or coke formation.[33,34] The effects of these compounds on the reactivity and lifetime of supported catalysts can be profound but have not yet been explored in detail for liquid-phase LA hydrogenation to GVL.

Herein, we report our studies on the performance and (long-term) stability of Ru-based catalysts in the presence of impurities in crude LA feeds. Impurity-free benchmark experiments (i.e., using reagent-grade LA) were first carried out using 1 wt % Ru/ZrO_2 and 1 wt % Ru/TiO_2 catalysts in both water and dioxane, at 90 and 150 °C, respectively. Catalyst performance during continuous-flow operation (i.e., with extended runtimes up to 190 h) was investigated, and the catalysts after the reaction were subsequently analyzed by N_2 physisorption, thermogravimetric analysis (TGA), transmission electron microscopy (TEM), and X-ray photoelectron spectroscopy (XPS). The influence of potential contaminants added individually to the reagent-grade LA feed on GVL productivity, and catalyst performance was tested in batch and continuous-flow setups. Impurities included (1) process-derived reagents and side-products (i.e., HCOOH, H_2SO_4, FFR, HMF, and humins) and (2) biogenic impurities such as amino acids (i.e., alanine, methionine, and cysteine). Catalyst characterization studies were carried out to provide insights into the relation between catalyst performance and catalyst structure. To the best of our knowledge, such systematic studies have not been reported in the literature.

EXPERIMENTAL SECTION

Materials. All chemicals were used as received without any further purification. Levulinic acid (>98%) and 1,4-dioxane (>99%) were purchased from Alfa Aesar; anisole (99%) from Acros Organics; formic acid and sulfuric acid (>95%) from Fisher Chemical; and furfural, 5-hydroxymethylfurfural, cysteine, methionine, methanol, and D_2O from Sigma-Aldrich. Ruthenium(III) nitrosyl nitrate ($RuNO(NO_3)_3$; Ru 31.3%) was obtained from Alfa Aesar, and

https://dx.doi.org/10.1021/acssuschemeng.9b07678
ACS Sustainable Chem. Eng. 2020, 8, 5903−5919

ZrO_2 (monoclinic, Daiichi Kikenso RC-100) and TiO_2 (P25) were obtained from Degussa. Acetone (>99%) was obtained from Interchema. Industrial humin samples were provided by Avantium, The Netherlands, and produced by conversion of fructose in methanol solvent. Both crude and purified humin samples were used for this study. The purified industrial humin was obtained by purification of a crude sample by solvent washing to remove residual monomeric HMF and 5-methoxymethylfurfural to values below 0.5 wt %. The purified industrial humin was obtained in the form of a dark brown-colored powder.

Catalyst Preparation. The Ru catalysts supported on ZrO_2 or TiO_2 (1 wt %) were prepared using a wet impregnation procedure as previously reported.[16] In a typical synthesis, the support was crushed and oven-dried for 2 h at 120 °C. The support was then dispersed in distilled water under stirring for 30 min. The precursor solution (10 mL, with the appropriate amount of precursor) was added dropwise to the suspended support. Subsequently, the mixture was stirred for 1 h. After removal of water under vacuum at 60 °C, the catalyst was dried in an oven at 60 °C overnight and heated at 500 °C for 3.5 h with a heating ramp of 5 °C min^{-1} under a N_2 flow of 100 mL min^{-1}, followed by its reduction in the same reactor at 450 °C for 5 h under a H_2 flow of 80 mL min^{-1}.

Catalytic Testing and Product Analysis. All batch reactions were performed in a 50 mL Parr batch autoclave at a temperature of 90 °C (water) or 150 °C (dioxane), a H_2 pressure of 50 bar, and a stirring speed of 1250 rpm. In a typical reaction, the batch autoclave reactor was loaded with the substrate (0.0258 mol LA), catalyst (0.75 g), and solvent (30 mL) (Table 1). The autoclave was then purged three times with argon, after which the reaction mixture was heated to the reaction temperature and charged with H_2. This was taken as the starting point of the reaction. During the reaction, samples were taken regularly and filtered with 0.2 μm PTFE filters in vials; then, 1 wt % anisole or dioxane was added as the internal standard, and the samples were diluted with dioxane or water prior to analysis. At the end of the reaction, the autoclave was submerged in ice-cold water to rapidly quench the reaction, after which the remaining H_2 was released. The catalyst was separated by filtration (filters of 0.45 μm), washed with acetone, and dried overnight at 60 °C in air. The reaction products were analyzed using a Shimadzu GC-2010A gas chromatograph equipped with a CPWAX 57-CB column (25 m × 0.2 mm × 0.2 μm) and a FID detector, using authentic samples for calibration. GC-MS measurements were performed on a Shimadzu GC-2010 using a VF5 ms column coupled to a Shimadzu GCMS-QP2010 mass spectrometer. High-performance liquid chromatography (HPLC) analysis was conducted using a Shimadzu LC-20AD HPLC equipped with a Bio-Rad Aminex HPX-87H column. H_2SO_4 (5 mM) at 60 °C with a flow rate of 0.55 mL min^{-1} was used as an eluent.

Recycling of the catalysts was performed by washing the spent catalysts recovered after the reaction with acetone and then by drying overnight at 60 °C. After the reaction, the gaseous products were collected in a gasbag and quantified using a micro-GC (Varian CP4900) chromatograph equipped with a COX column and a TCD detector. The concentration of HCOOH was determined by HPLC equipped with a refractive index detector at 60 °C with a dilute aqueous H_2SO_4 solution (5 mM) as the mobile phase at a flow rate of 0.55 mL min^{-1}. The composition of the reaction mixture in water was determined by HPLC as well as ^1H NMR, which was previously shown to be the best method to quantify the intermediate 4-hydroxypentanoic acid (4-HPA). A sample (200 μL) was weighed and dissolved in D_2O, and dioxane (methanol as the internal standard, 10 μL) was added to the sample.

The continuous-flow setup consisted of a feeding section, a fixed bed reactor, a gas–liquid separator, and a fraction collector. The fixed bed reactor was a 5 cm long 1/4″ outer diameter stainless steel tube with an internal diameter of 3.6 mm. The bed was held in place on both ends by paper filters supported by a metal grid. The liquid was fed to the reactor using an HPLC pump, the gas flow was controlled by a mass-flow controller. Gas and liquid were passed through separate coils of tubing to heat the flows before they entered the reactor. Both flows were mixed just before entering the reactor. The reactor and heating coils were placed in a temperature-controlled convection oven to maintain a constant temperature and to allow for isothermal operation. The pressure was kept constant with the use of a back-pressure regulator. After the back-pressure valve, the gas and liquid flow were separated by a gas–liquid separator. A fraction collector robot was used to collect the liquid at specified time intervals.

The stability of the 1 wt % Ru/TiO_2 and 1 wt % Ru/ZrO_2 catalysts was tested in water and dioxane by performing runs with extended times on the stream. The conditions for the continuous-flow LA hydrogenation experiments with or without added impurities are summarized in Table 2. The experiments were performed at 90 °C for water and 150 °C for dioxane to compensate for the catalyst's intrinsically far higher activity in water than in dioxane. The weight hourly space velocity (WHSV) was used to steer the LA conversion at a conversion level between 80 and 90% (and not higher) to obtain reliable data for catalyst deactivation. Experiments were performed with a starting solution of 10 wt % LA in either water or dioxane. In a typical run, the reactor was filled with 100 mg of catalyst mixed with sufficient SiC to fill the reactor completely. The hydrogen pressure for all experiments was 50 bar, and a hydrogen flow of 35 N mL min^{-1} was used. The molar excess ratio of hydrogen to LA varied

Table 1. Experimental Conditions for Batch LA Hydrogenation Experiments with and without Impurities

conditions	dioxane	water
catalyst (1 wt % Ru)	Ru/ZrO_2	Ru/TiO_2
Ru/LA wt ratio (without impurities)	2000	2000
Ru/LA molar ratio (with impurities)	400	400
temperature (°C)	150	90
hydrogen pressure (bar)	50	50
reaction time (min)	300	300
volume of solvent (mL)	30	30

Table 2. Experimental Conditions for Continuous-Flow LA Hydrogenation Experiments with and without Impurities

conditions	dioxane	water
runs without impurities		
catalyst (1 wt % Ru)	Ru/ZrO_2 or Ru/TiO_2	Ru/ZrO_2 or Ru/TiO_2
LA inlet concentration (wt %)	10	10
catalyst amount (mg)	100	100
temperature (°C)	150	90
hydrogen pressure (bar)	50	50
WHSV (g_{feed} g_{cat}^{-1} h^{-1})	2.4	3.6
time-on-stream (h)	190	190
runs with impurities		
added impurity	HCOOH, H_2SO_4, or FFR	HCOOH, H_2SO_4, or FFR
catalyst (1 wt % Ru)	Ru/ZrO_2 or Ru/TiO_2	Ru/ZrO_2 or Ru/TiO_2
LA inlet concentration (wt %)	10	10
impurity concentration (wt %)	0.5	0.5
catalyst amount (mg)	100	100
		200 (Ru/ZrO_2/HCOOH, $Ru/ZrO_2/H_2SO_4$)
temperature (°C)	150	90
hydrogen pressure (bar)	50	50
WHSV (g_{feed} g_{cat}^{-1} h^{-1})	1.7	3.6
		0.9 (Ru/ZrO_2/HCOOH)

https://dx.doi.org/10.1021/acssuschemeng.9b07678
ACS Sustainable Chem. Eng. 2020, 8, 5903−5919

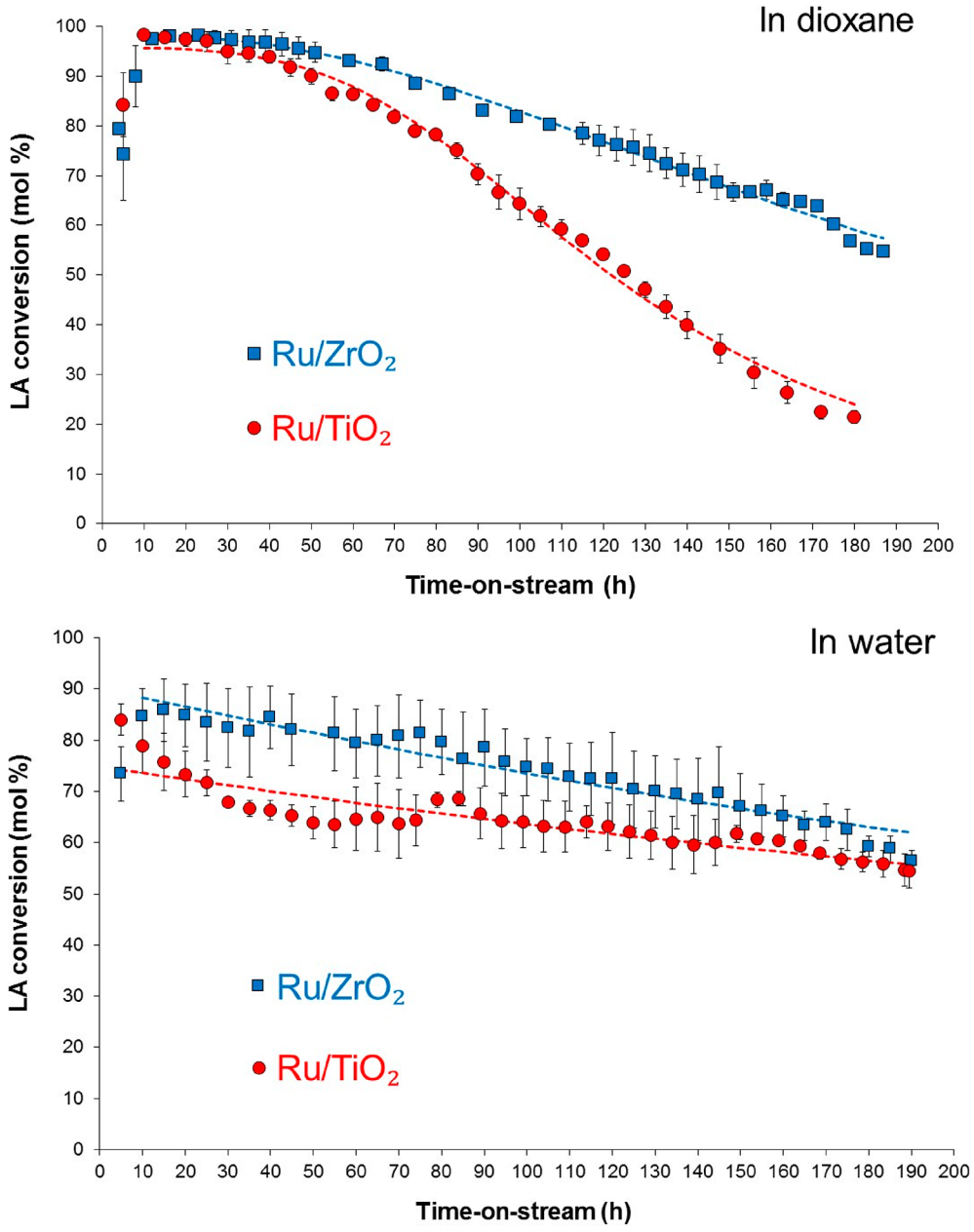

Figure 1. Comparison of the long-term stability between 1 wt % Ru/ZrO_2 and 1 wt % Ru/TiO_2 catalysts in water and dioxane. Average LA conversions are given as a function of time-on-stream for the hydrogenation of reagent-grade LA to GVL in a continuous-flow setup in dioxane (WHSV 2.4 h^{-1}, 50 bar H_2, 150 °C) and water (WHSV 3.6 h^{-1}, 50 bar H_2, 90 °C). Dashed lines refer to the modeled LA conversion at the reactor exit (*vide infra*).

between 30 and 60 depending on the WHSV. The oven was set at 90 °C for the experiments in water and at 150 °C for experiments in dioxane. The concentrations of LA, GVL, and 4-HPA in the collected fractions were determined by ^1H NMR with dioxane as the internal standard in the case of the experiments in water and methanol in the case of dioxane. Long duration catalytic runs were performed with a feed containing only reagent-grade LA and solvent. A typical run with contaminants consisted of running the setup for 24 h with reagent-grade LA/solvent only, followed by a period of 24 h where the feed was switched to LA/solvent/0.5 wt % contaminant. After this period, the feed was switched back to the original LA/solvent solution for 24 h.

Catalyst Characterization. Thermal gravimetric analysis (TGA) was performed on a PerkinElmer Pyris 1 apparatus. Typically, the sample was initially heated to 200 °C for 1 h with a temperature ramp of 10 °C min^{-1} in a 20 mL min^{-1} flow of Ar to exclude physisorbed water and acetone, followed by a ramp of 5 °C min^{-1} to 600 °C in a 10 mL min^{-1} flow of air to burn off any organic deposits formed. N_2 physisorption isotherms were recorded to determine surface areas and pore volumes with a Micromeritics Tristar 3000 setup operating at −196 °C. The samples were outgassed prior to performing the measurement for 20 h at 300 °C in a N_2 flow. Surface areas were determined using the Brunauer−Emmett−Teller (BET) theory, while micropore volumes (cm^3 g^{-1}) were determined by *t*-plot analysis for *t* between 3.5 and 5.0 Å to ensure inclusion of the minimum required pressure points. TEM measurements were conducted in the bright-field imaging mode by using a Tecnai 20FEG transmission electron microscope operated at 200 kV. X-ray photoelectron spectroscopy (XPS) measurements were carried out on a Thermo Scientific K-Alpha spectrometer, equipped with a monochromatic small-spot X-ray source and a 180° double-focusing hemispherical analyzer with a 128-channel detector. Spectra were

https://dx.doi.org/10.1021/acssuschemeng.9b07678
ACS Sustainable Chem. Eng. 2020, 8, 5903−5919

Table 3. Physicochemical Properties of the Fresh and Spent 1 wt % Ru/TiO_2 and 1 wt % Ru/ZrO_2 Catalysts after Long-Term Stability Experiments in a Continuous-Flow Set-up Using Reagent-Grade LA

Ru catalyst		solvent	BET surface area (m^2 g^{-1})	total pore volume (cm^3 g^{-1})	BJH desorption average pore diameter (nm)	average Ru particle size (nm)	average wt loss (%)[b]
Ru/TiO_2	fresh	NA[a]	75	0.31	15	2.6 ± 1.4	NA
	spent	dioxane	48	0.42	32	3.2 ± 1.3	3.2
	spent	water	67	0.52	26	3.0 ± 0.7	2.8
Ru/ZrO_2	fresh	NA	94	0.26	9.5	clear particles not observed	NA
	spent	dioxane	94	0.25	9.3	2.3 ± 0.8	4.6
	spent	water	73	0.20	9.8	2.9 ± 1.1	8.9

[a]NA means not applicable. [b]TGA.

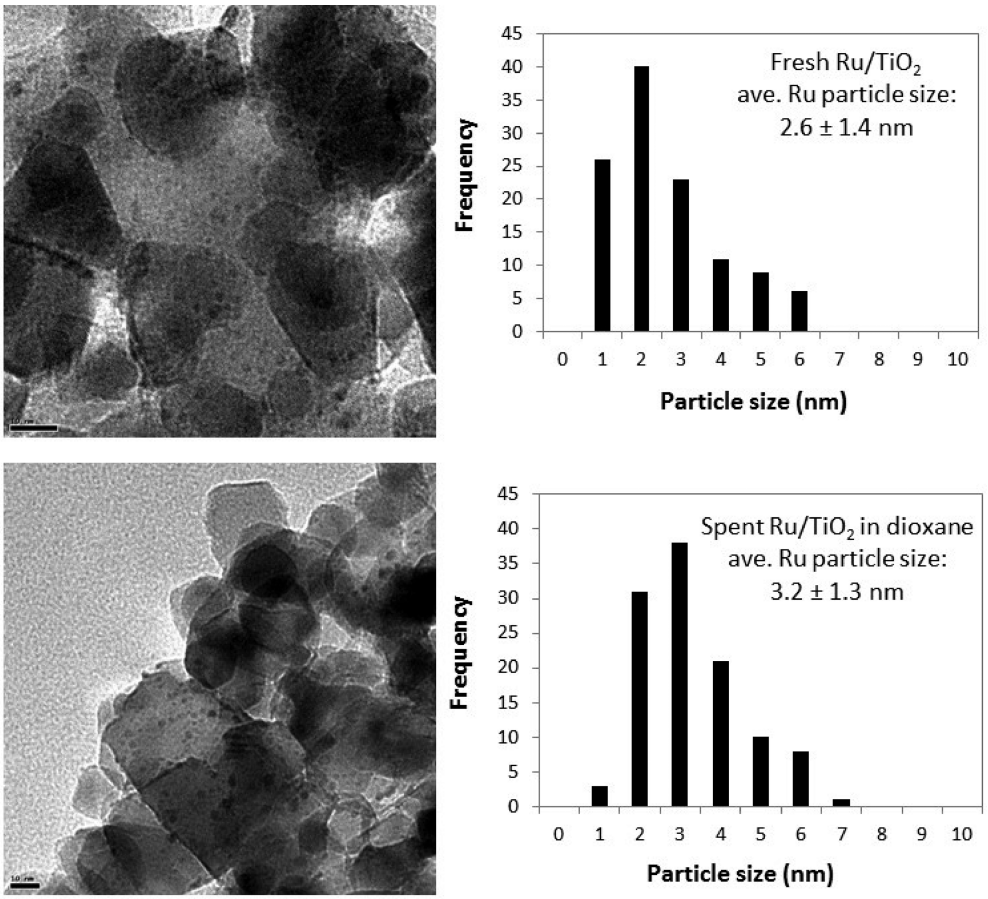

Figure 2. Representative TEM images and average Ru particle size and distribution for (top) fresh and (bottom) spent 1 wt % Ru/TiO_2 catalyst in dioxane after long-term stability experiments in a continuous-flow setup using reagent-grade LA.

obtained using an aluminum anode ($h\nu$(Al Kα) = 1486.6 eV) operating at 72 W and a spot size of 400 μm. The background pressure of the UHV chamber was 2×10^{-8} mbar. Survey scans were measured at a constant pass energy of 200 eV and region scans at 50 eV. Due to the differential charging of Ru/TiO_2 samples, binding energy (BE) calibration was performed by setting the Ru $3d_{5/2}$ peak of the Ru metal to 280.0 eV. ZrO_2-supported catalysts were BE-calibrated by setting the C 1s signal of sp^3 adventitious carbon to 284.8 eV.

RESULTS AND DISCUSSION

Benchmark Experiments in a Continuous-Flow Reactor: Hydrogenation of LA without Impurities. The performance and particularly the long-term stability of the Ru/ZrO_2 and Ru/TiO_2 catalysts were initially tested in a continuous-flow reactor in both water and dioxane, providing a baseline for comparison with the experiments involving impurities. The LA conversion was ensured to be below 100% to allow for a proper assessment of long-term stability (see Table 2 for experimental details). Experiments were conducted at least in duplicate and average values with confidence intervals are given. In all cases, the only products were GVL and 4-HPA; possible overhydrogenation products (e.g., valeric acid and 1,4-pentanediol) were not observed (HPLC, GC).

Experiments in Dioxane. For experiments in dioxane at 150 °C, the initial LA conversion for both catalysts was found between ~70−90 mol % (Figure 1). A clear increase in LA conversion was observed in the first 10 h on-stream. This increase in catalytic activity suggests the occurrence of *in situ* activation of the catalysts (*vide infra*). The activity of both catalysts was comparable after 24 h on-stream. However, a considerable drop in activity was observed for extended times

https://dx.doi.org/10.1021/acssuschemeng.9b07678
ACS Sustainable Chem. Eng. 2020, 8, 5903−5919

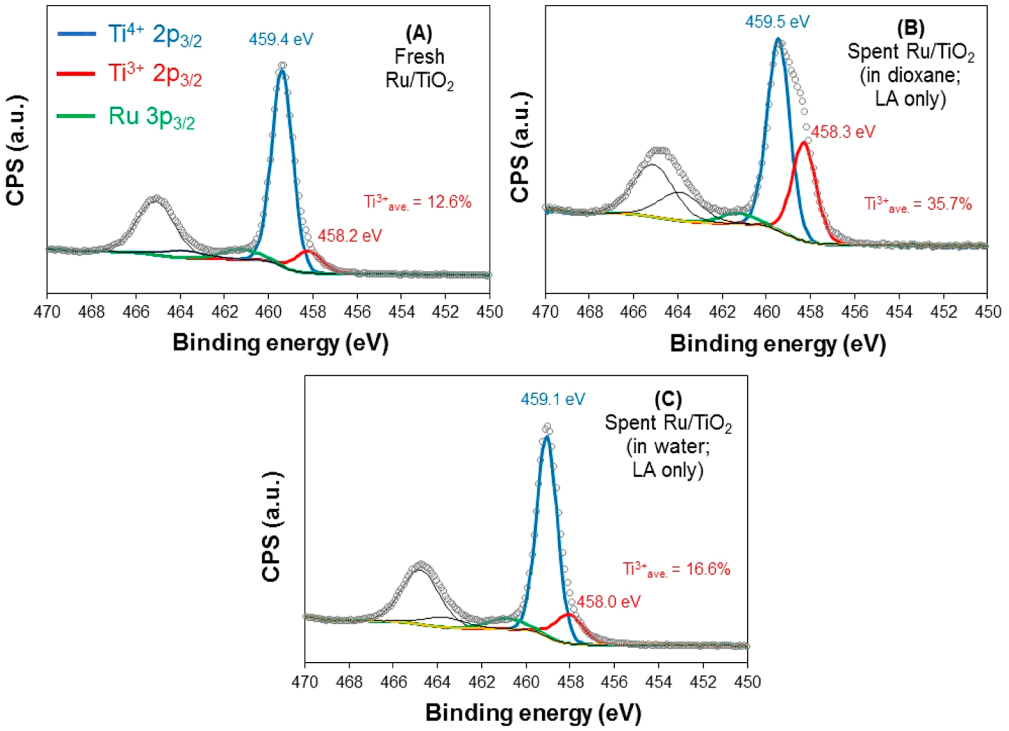

Figure 3. Ti^{4+} $2p_{3/2}$ and Ti^{3+} $2p_{3/2}$ XP spectra of (A) fresh and (B and C) spent 1 wt % Ru/TiO_2 catalysts after long-term stability experiments in a continuous-flow setup using reagent-grade LA in dioxane and water. Corresponding O 1s XP spectra are presented in Figure S1.

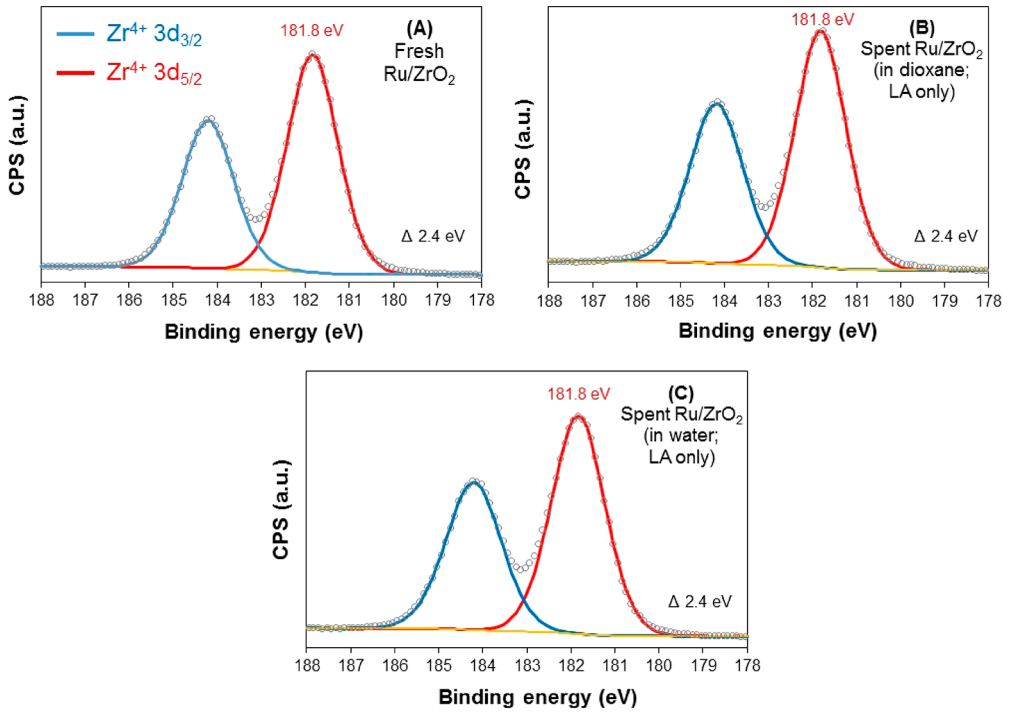

Figure 4. Zr^{4+} $3d_{3/2}$ and Zr^{4+} $3d_{5/2}$ XP spectra of (A) fresh and (B and C) spent 1 wt % Ru/ZrO_2 catalysts after long-term stability experiments in a continuous-flow setup using reagent-grade LA in dioxane and water. Corresponding O 1s XP spectra are presented in Figure S3.

on-stream (>60 h). The Ru/ZrO_2 catalyst proved to be more stable in dioxane than its TiO_2 analogue. To understand these differences in stability, the physicochemical properties of fresh and spent catalysts after each 190 h run were determined by N_2 physisorption, TGA, TEM, and XPS. For dioxane experiments with Ru/TiO_2, deactivation is at least partly caused by a reduction in the specific surface area from 75 to 48 m^2 g^{-1} (Table 3). Furthermore, the average pore diameter for Ru/TiO_2 increased significantly from 15 to 32 nm. In addition, TGA analysis of the spent catalyst showed a 3.2% weight loss, suggesting some deposition of carbonaceous material on the catalyst surface. Deactivation of the Ru/TiO_2 catalyst in dioxane is not caused by the sintering of Ru nanoparticles (Figure 2), with the average Ru nanoparticle

https://dx.doi.org/10.1021/acssuschemeng.9b07678
ACS Sustainable Chem. Eng. 2020, 8, 5903−5919

diameter of the spent catalyst not having changed significantly. However, XPS measurements suggest that support reduction may play a role in catalyst deactivation. Figure 3 shows that the fresh catalyst contains mostly TiO_2 with Ti^{4+} species at the surface, as indicated by the intense Ti^{4+} $2p_{3/2}$ component centered at 459.4 eV.[35] A small contribution of Ti^{3+} species (12.6%; 458.2 eV) is also present.[35] In comparison, the spent catalyst showed a large increase in the relative amount of Ti^{3+} species (35.7%; 458.3 eV). Fresh Ru/TiO_2 showed a Ti^{4+}/Ti_{total} ratio of 87%, which decreased to 64% for the spent catalyst after reaction in dioxane. In agreement with this, the O 1s features of fresh and spent catalysts are also different, showing that the relative proportion of $O-Ti^{4+}$ has been reduced to $O-Ti^{3+}$ (Figure S1). These findings suggest that deactivation of Ru/TiO_2 is related to the partial reduction of the TiO_2 support,[36] consistent with our previous findings in batch recycling studies.[16]

The greater stability of the Ru/ZrO_2 catalyst in dioxane is reflected in the more minor changes in textural properties, including BET surface area and average pore volume (Table 3). TEM analysis of spent Ru/ZrO_2 shows the presence of Ru nanoparticles (average size of 2.3 ± 0.8 nm), whereas distinct nanoparticles could not be detected in the fresh catalyst (Figure S2). The fresh Ru/ZrO_2 catalysts are assumed to be atomically dispersed.[16] As such, some Ru restructuring of the catalyst by redispersion of ruthenium happened at early times on-stream, a process implicated in the increase in catalytic activity seen during this phase (i.e., *in situ* activation).

The TGA analysis of the spent Ru/ZrO_2 catalyst showed the presence of some carbonaceous material (4.6%), suggesting that coke build-up may contribute to the gradual decrease in activity in dioxane. The XPS analysis did not show any evidence of ZrO_2 support reduction (Figure 4). For example, fresh Ru/ZrO_2 showed the typical the Zr^{4+} 3d spectra with spin−orbit doubles ($3d_{5/2}$ and $3d_{3/2}$) separated by 2.4 eV.[35] The XP spectra for the spent Ru/ZrO_2 do not show any significant intensity change or any spectral features indicative of ZrO_2 reduction after the reaction. However, when comparing the O 1s XP spectra for fresh and spent Ru/ZrO_2, an obvious increase in the relative proportions of O species exposed on or near the surface of the catalyst was observed for the latter catalyst (Figure S3).[37,38] This suggests the deposition of organic compounds and/or an increase in hydroxyl groups on the catalyst surface after the reaction.

Experiments in Water. Because the LA hydrogenation activity of Ru catalysts is known to be higher in water than in dioxane, a lower reaction temperature of 90 °C was used for the continuous-flow experiments in this solvent. The activity profiles of the two catalysts versus time-on-stream are also given in Figure 1, and the details regarding the experimental conditions are summarized also in Table 2. In general, both catalysts proved to be more stable in water than in dioxane under the adopted reaction conditions. In addition to the solvent effects on stability, this observation could also be due to differences in the reaction temperature used (90 °C for water vs 150 °C for dioxane). For Ru/ZrO_2, again, an increase in activity is seen in the first 10 h of the run, likely due to a slight increase in the Ru nanoparticle size, which is also observed for the runs in dioxane. This phenomenon is rationalized by our earlier investigations on Ru-based catalysts for LA hydrogenations, showing an optimum in regards to the catalytic activity versus the average nanoparticle size (about 2−3 nm).[20] After this, a gradual drop in the activity was found. The TiO_2-supported catalyst showed a gradual decrease over the entire run, again without showing the initial increase in activity, as seen in dioxane. The deactivation rates for both catalysts in water are rather similar, but kinetic modeling showed the TiO_2-supported catalyst to be slightly more stable (*vide infra*).

The physicochemical characterization of the spent Ru/ZrO_2 catalyst suggested the major cause for catalyst deactivation to be the formation of carbonaceous deposits, as evidenced by a weight loss of 9% during TGA. These deposits are also held responsible for the reduction in BET surface area (94 to 73 $m^2\ g^{-1}$) and total pore volume (0.26 to 0.20 $cm^3\ g^{-1}$). Partial deactivation due to the reduction of the ZrO_2 support is not likely, as evidenced by the lack of change in the XPS peak signatures (Figure 4). In contrast to Ru/ZrO_2, the observed deactivation profile for Ru/TiO_2 is likely caused by a combination of effects. For example, TGA analysis of the spent Ru/TiO_2 catalyst shows a weight loss of 2.8%, indicating the formation of a minor amount of carbonaceous material on the surface. Moreover, the XPS measurements showed that the relative quantity of Ti^{4+} species on the surface is reduced slightly after the run in water (e.g., Ti^{4+}/Ti_{total} ratio of 87% for fresh catalyst is reduced slightly to 83% after the reaction) (Figure 3). TEM measurements performed on both fresh and spent Ru/TiO_2 catalysts show statistically similar values (2.6 ± 1.4 nm and 3.0 ± 0.7 nm) (Figure S2), excluding metal sintering as a major cause of deactivation.

Quantification of Catalyst Deactivation. Many different models for deactivation kinetics have been proposed.[39,40] Usually, these models assume the deactivation kinetics and reaction kinetics to be separable. This allows the activity, $a(t)$, to be defined as the ratio of the actual rate and the initial rate, $a = r/r_0$. The observed long-term catalyst stability profiles, presented in Figure 1, show different rates of deactivation that depend on the catalyst support and the solvent that was used in the experimental runs. As shown in Figure 1, the observable is the conversion, x, at the exit of the reactor. In order to quantify the activity, it must be related to the observed conversions. This activity−conversion relationship depends on the reactor configuration and the reaction kinetics but not on the actual deactivation kinetics. For example, the simple relationship $a = x/x_0$, which assumes that the activity equals the ratio of the exit conversion to the initial exit conversion, is valid only for zero-order reactions.

A simple, empirical model for the decrease of the catalyst activity with time is

$$a = \frac{1}{1 + k_d t^m} \tag{1}$$

Equation 1 can describe the deactivation due to different phenomena (e.g., sintering of the active metal components or coking or fouling of the catalyst).[40] In this work, we used this equation to describe the deactivation behavior of the catalysts by optimizing the parameters k_d and m of the model. The results are shown in Table 4 below.

The results of the model development are illustrated in Figure 1. In establishing the activity−conversion relationship in this case, first-order reaction kinetics were assumed and any axial or radial dispersion effects in the packed bed were neglected. The fit between the model and experimental data is good, as seen in Figure 1. The modeled deactivation constants in water imply that the TiO_2-supported Ru catalyst is slightly more stable than the ZrO_2 analogue. The model parameters

https://dx.doi.org/10.1021/acssuschemeng.9b07678
ACS Sustainable Chem. Eng. 2020, 8, 5903−5919

Table 4. Calculated Parameters of the Deactivation Model Equation 1

	parameter	Ru/ZrO_2	Ru/TiO_2
dioxane	k_d	7.94×10^{-4}	5.55×10^{-6}
dioxane	m	1.64	2.78
water	k_d	7.26×10^{-3}	3.67×10^{-3}
water	m	1	1

may be used for, among others, the design of suitable reactor configurations and for an estimation of the variable catalyst costs for the hydrogenation reaction.

Influence of Reagents and Side-Products from LA Synthesis on Catalyst Performance. Experiments with impurities were carried out using the same Ru catalysts in both water and dioxane. Brønsted acid impurities included HCOOH, an inevitable byproduct of LA production from C6 sugar sources, and H_2SO_4, a typical example of a mineral acid catalyst used for LA synthesis. Furfural, 5-hydroxymethylfurfural, and humins can be expected to be present in (trace) amounts as intermediates and byproducts of LA synthesis. Finally, amino acids can potentially be present in the LA feed when nonlignocellulosic biomasses are used (e.g., from proteins in press-cake residues from oil-seed processing units). Cysteine and methionine were tested as sulfur-functional groups, which are particularly detrimental for Ru-based nanoparticle catalysts.

Influence of Formic Acid. The effect of HCOOH on catalytic performance was initially explored in a continuous-flow setup. Initially, the reactor was fed with 10 wt % LA for about 24 h, after which the feed was switched to a solution containing 10 wt % LA and 0.5 wt % HCOOH. After, again, about 24 h, the feed was switched back to the LA-only solution, and the experiment was continued for up to about 50 h. For all four runs (Ru/TiO_2 and Ru/ZrO_2 in both water and dioxane), the profiles of the first 24 h of operation (LA only, no impurities) were in line with the benchmark experiments and showed high LA conversion and selectivity to GVL (Figure 5). *In situ* activation was again observed for the Ru/ZrO_2 catalyst. A severe drop in catalytic activity was seen when HCOOH was introduced in the LA feed, showing full loss of activity on a time scale of hours. Of interest is the difference in response to the addition of HCOOH when considering the support type. For the ZrO_2-supported Ru catalyst in both solvents, the activity remains constant until about 5 h after HCOOH addition and then rapidly drops to zero. For the TiO_2-supported Ru catalyst, the response is much faster, and directly after HCOOH addition in the LA feed, a drop in catalytic activity is observed.

Remarkably, when the feed is switched back to reagent-grade LA after about 48 h, the catalysts regained activity, and the values based on the benchmark experiments, taking into account the expected extent of deactivation, are retained. These findings show that while HCOOH addition to LA does lead to deactivation, reactivation of the catalysts is possible. A plausible explanation for this is the preferential adsorption of HCOOH instead of LA to the Ru nanoparticles, followed by conversion of the formic acid on the Ru catalyst to give mixtures of (adsorbed) CO, CO_2, and H_2.[41] Dehydrogenation and dehydration pathways of HCOOH are well-established in the literature, particularly for Ru catalysts. In fact, HCOOH is often used as an internal hydrogen source as well as in the LA hydrogenation using Ru/C catalysts.[42−44] In this present work, however, the coproduced CO may strongly adsorb on the Ru nanoparticles and possibly poison the catalysts.[41,45,46] Spent catalysts after each run were analyzed, and the results are summarized in Table 5.

Changes in textural properties for both Ru/ZrO_2 and Ru/TiO_2 catalysts after the runs in water were comparable with the benchmark experiments performed with LA only. Small differences are attributed to the differences in the cumulative run times (190 h for benchmark vs a maximum of 90 h for runs with added HCOOH). In general, the weight loss recorded by TGA of spent catalysts was higher for Ru/ZrO_2 than for Ru/TiO_2. On the other hand, XPS measurements of spent Ru/TiO_2 in water showed an increased proportion of surface Ti^{3+} (e.g., Ti^{4+}/Ti_{total} of 76% from 83% without HCOOH) (Figure 6) and stoichiometric TiO_2 (Figure S4), implying that the presence of HCOOH in LA hydrogenation enhances TiO_2 reduction.

Additional experiments in a batch setup were performed with and without HCOOH present at the start of the reaction, and the results are consistent with those obtained in the continuous-flow setup. Figure 7 shows the performance of Ru/ZrO_2 in the presence of various amounts of HCOOH in dioxane (benchmark batch experiments with LA only are presented in Figures S5 and S6). In the presence of HCOOH, the initial activity for LA hydrogenation is zero. After a certain induction period, the catalyst becomes active for LA hydrogenation and GVL is formed. The induction period is a function of the HCOOH/LA molar ratio, with higher ratios leading to longer induction times. Using an equimolar amount of HCOOH to LA, the LA conversion to GVL is only 2% after 360 min of reaction; however, the conversion of HCOOH is already at 75% (Figure S7). Interestingly, even all HCOOH was converted after extended batch times for HCOOH/LA mole ratios higher than 8 (Figure S8). These findings suggest that HCOOH is reacting far more rapidly than LA, most probably to gas phase components. Once the HCOOH is converted, the subsequent hydrogenation of LA occurs. To confirm this, the reactivity of HCOOH over Ru/ZrO_2 in dioxane in the absence of LA and external H_2 was examined at a concentration of 26 mmol (equivalent to a run with a 1:1 HCOOH/LA mole ratio) at 150 °C. Gas analysis by GC-TCD after a reaction of 180 min indeed showed the formation of H_2, CO_2, and small amounts of CO (Table S1).

The observed reversible inhibition by HCOOH is therefore due to the preferred adsorption of HCOOH on the Ru surface, possibly combined with CO poisoning of the Ru active sites, followed by the conversion of the HCOOH to gas phase components. Inhibition is fully reversible, as was demonstrated by the five-times consecutive reuse of the Ru/ZrO_2 catalyst in runs with a 1:8 HCOOH/LA mole ratio, followed by washing the spent catalyst with acetone and mild drying (60 °C), showing no loss in activity or selectivity (Figure S9). These findings are in agreement with the experiments performed in the continuous-flow reactor setup.

For comparison, the catalytic batch experiments were also performed in water (90 °C) in the presence of various amounts of HCOOH (Figure 8). Similar effects as found in dioxane were observed, which were also in line with the continuous-flow experiments. The negative effect of HCOOH on catalyst activity is significantly more pronounced in water than in dioxane (e.g., at 1:20 HCOOH/LA for Ru/ZrO_2). In fact, HCOOH is still present in water after 180 min batch

https://dx.doi.org/10.1021/acssuschemeng.9b07678
ACS Sustainable Chem. Eng. 2020, 8, 5903−5919

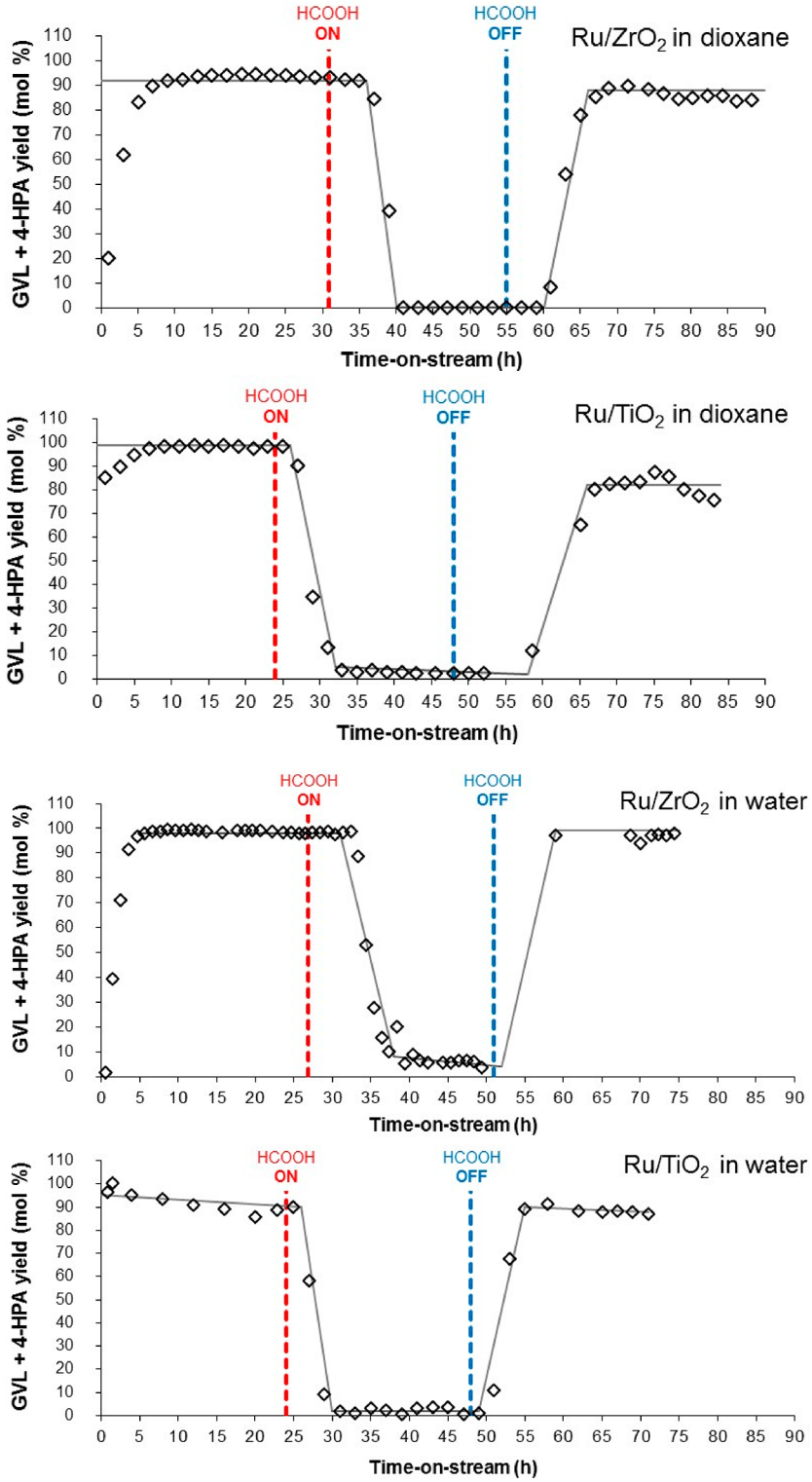

Figure 5. Influence of formic acid on LA hydrogenation activity. Combined GVL and 4-HPA yields are given as a function of time-on-stream in a continuous-flow setup using 1 wt % Ru/ZrO_2 and 1 wt % Ru/TiO_2 catalysts in dioxane (150 °C) and water (90 °C).

reaction time (9%), whereas it is already fully converted at this point for reactions in dioxane.

Influence of Sulfuric Acid. Similar to the HCOOH-spiked experiments in the continuous-flow setup, the effect of H_2SO_4 on LA hydrogenation was tested by running LA (10 wt %) for 24 h, followed by a combined feeding of LA (10 wt %) and H_2SO_4 (0.5 wt %) for 24 h, and finally back to feeding LA (10 wt %) for the remainder of the run (Table 2). Typically, the total time on-stream was 75 h. As shown in Figure 9, the addition of H_2SO_4 led to distinct differences in performance between both solvents observed for both catalysts. In dioxane, the catalytic activity remained constant for about 8 h after starting the LA/H_2SO_4 feed and then dropped to less than 10% of the original value. Upon switching back to the LA

https://dx.doi.org/10.1021/acssuschemeng.9b07678
ACS Sustainable Chem. Eng. 2020, 8, 5903−5919

Table 5. Physicochemical Properties of the Fresh and Spent 1 wt % Ru/TiO_2 and 1 wt % Ru/ZrO_2 Catalysts after Long-Term Stability Experiments in a Continuous-Flow Set-up Using LA in the Presence of Impurities

Ru catalyst type	solvent	impurity	BET surface area ($m^2\ g^{-1}$)	total pore volume ($cm^3\ g^{-1}$)	BJH desorption average pore diameter (nm)	average wt loss (%)[b]
fresh Ru/TiO_2	NA[a]	NA	75	0.31	15	NA
spent Ru/TiO_2	water	HCOOH	53	0.44	29.8	2
spent Ru/TiO_2	water	H_2SO_4	50	0.41	30.1	1
spent Ru/TiO_2	water	furfural	48	0.41	29.4	1
fresh Ru/ZrO_2	NA	NA	94	0.26	9.5	NA
spent Ru/ZrO_2	water	HCOOH	90	0.28	10.2	4
spent Ru/ZrO_2	dioxane	HCOOH	76	0.26	10.9	3.7
spent Ru/ZrO_2	water	H_2SO_4	74	0.22	9.7	3
spent Ru/ZrO_2	dioxane	H_2SO_4	85	0.27	11.4	3.03
spent Ru/ZrO_2	water	furfural	82	0.24	9.9	2.03
spent Ru/ZrO_2	dioxane	furfural	90	0.30	10.7	3.45

[a]NA means not applicable. [b]TGA.

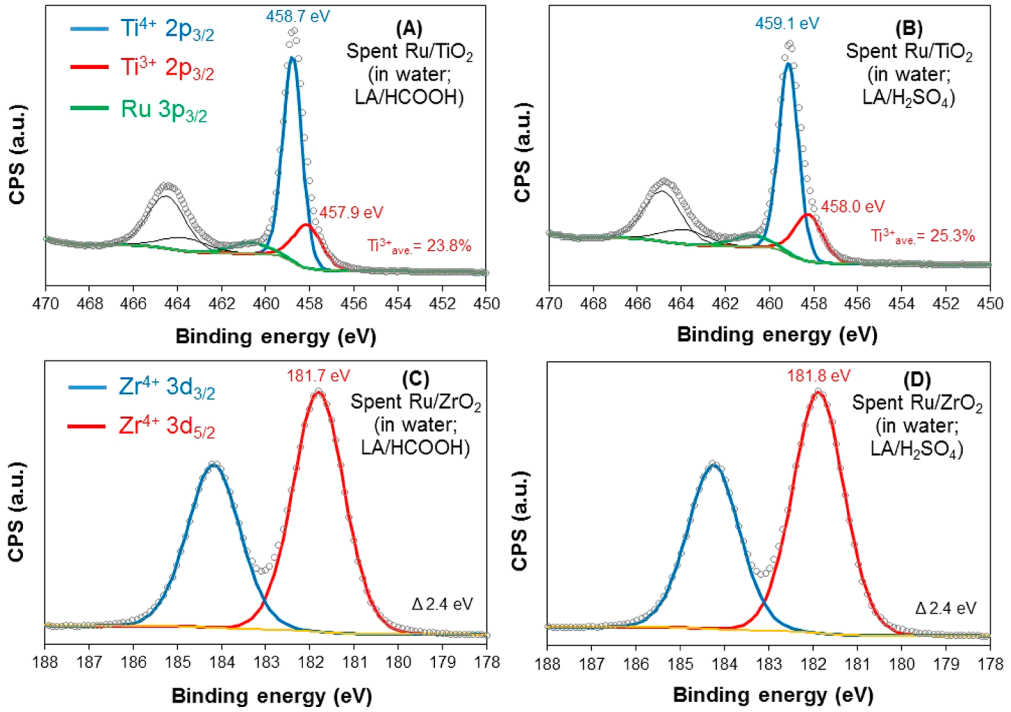

Figure 6. (A and B) Ti^{4+} $2p_{3/2}$ and Ti^{3+} $2p_{3/2}$ and (C and D) Zr^{4+} $3d_{3/2}$ and Zr^{4+} $3d_{5/2}$ XP spectra of spent 1 wt % Ru/TiO_2 and 1 wt % Ru/ZrO_2 catalysts after long-term stability experiments in a continuous-flow setup using LA in the presence of impurities in dioxane and water. Corresponding O 1s XP spectra are presented in Figure S4.

feed, the catalytic activity remained at the low level, and the original level was not regained. These findings indicate that irreversible deactivation occurred, most likely by sulfur poisoning of the active Ru nanoparticles. Such deactivation behavior has been observed in the literature for Ru-based catalysts. For example, sulfur-containing impurities can adsorb strongly on metal surfaces and prevent the further adsorption of reactant molecules, leading to substantial or complete loss of activity.[31,47] The exact influence of a sulfur-containing impurity on a Ru-based catalyst will strongly depend on the oxidation and protonation state of the sulfur-containing potential poison and its ease of reduction under the applied reaction conditions. Previous studies have revealed that surface sulfates can be reduced into sulfides under reductive and acidic conditions,[48] which eventually react, forming Ru sulfides and sulfates, and poison the Ru active surface.

Of interest is the observed delay in deactivation of the catalyst upon switching to the LA/H_2SO_4 feed, suggesting that the oxidic supports are capable of binding a certain amount of SO_4^{2-} anions before these are detrimental to catalyst activity. This finding is in line with our previous experiments in batch setups using dioxane as the solvent and Ru/ZrO_2 as the catalyst.[31] Examination of the spent Ru/ZrO_2 catalyst by ICP after the 75 h reaction with H_2SO_4 in the LA feed indeed showed the presence of sulfur (1.82 wt % S based on sample weight). Sulfur poisoning is thus an important cause of Ru catalyst deactivation and is in line with an expected depletion of the scavenging capacity of the support, as shown above. However, irreversible deactivation may be prevented or delayed by adopting a suitable regeneration method (i.e., hot water wash) and timely regeneration cycles.[31]

In water, the yield versus time-on-stream profiles are distinctly different from those in dioxane. Upon switching to

https://dx.doi.org/10.1021/acssuschemeng.9b07678
ACS Sustainable Chem. Eng. 2020, 8, 5903−5919

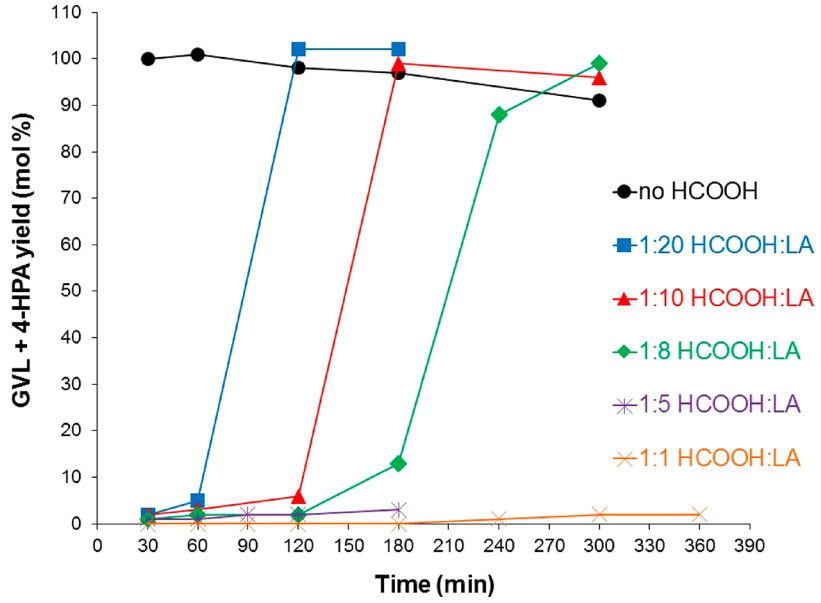

Figure 7. Influence of formic acid on LA hydrogenation activity. Combined GVL and 4-HPA yields are given as a function of time in a batch setup using a 1 wt % Ru/ZrO_2 catalyst in dioxane in the presence of formic acid at different mole ratios with LA. Conditions: LA/Ru wt ratio of 400, 150 °C, and 50 bar H_2.

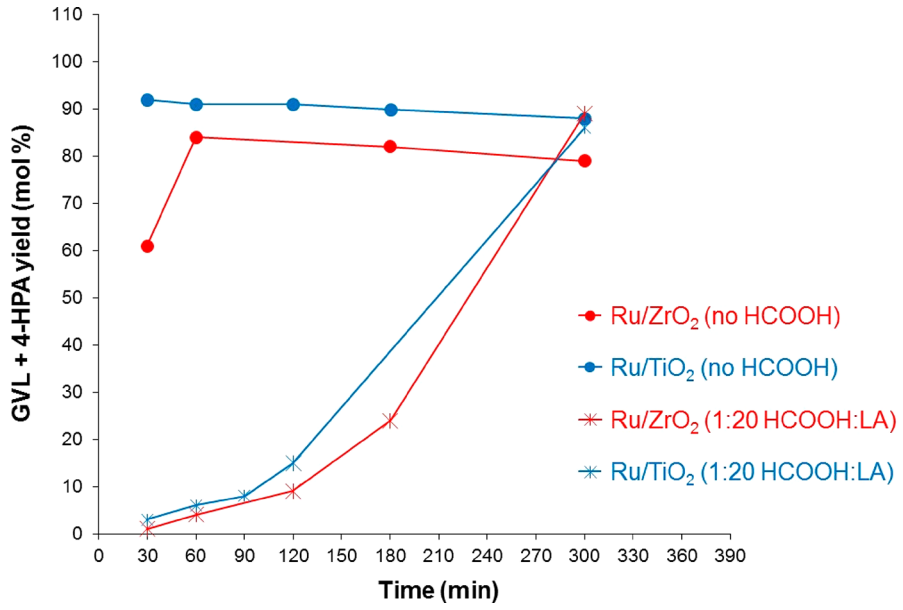

Figure 8. Influence of formic acid on LA hydrogenation activity. Combined GVL and 4-HPA yields as a function of time in a batch setup using 1 wt % Ru/ZrO_2 and 1 wt % Ru/TiO_2 catalysts in water in the presence of formic acid at 1:20 mol ratios. Conditions: LA/Ru wt ratio of 400, 90 °C, and 50 bar H_2.

the LA/H_2SO_4 feed, an immediate loss in activity was observed; however, the drop in catalytic activity was much less than for experiments in dioxane. After switching back to the reagent-grade LA, the activity remained about constant. As such, irreversible deactivation occurs, likely again due to sulfur poisoning of the active Ru sites. However, the rate of deactivation is by far less than for experiments in dioxane, most likely due to the difference in temperature and scavenging efficiency. Spent catalysts were analyzed, and the results are given in Table 5. Generally, changes in textural properties for both Ru/ZrO_2 and Ru/TiO_2 after the runs in water were comparable with the benchmark experiments performed with LA only. Coke build up in spent catalysts is also relatively limited (1−3%), suggesting that fouling is not the major cause of deactivation. A Ti^{4+}/Ti_{total} % ratio of 75% was measured for the spent Ru/TiO_2 run in water (from 83% using LA only), which is comparable to those recorded for the spent catalyst with HCOOH (76%) (Figure 6).

Influence of Furfural, 5-Hydroxymethylfurfural, and Industrial Humins. Flow experiments using the same catalysts and solvents were performed to determine the effect of FFR on LA hydrogenation activity. The profiles of the first 24 h of operation using impurity-free LA were in line with the benchmark experiments for all four runs (Figure 10). Upon FFR addition (0.5 wt %), the catalytic activity slowly declined. Nonetheless, when switching back to a pure LA feed after the

https://dx.doi.org/10.1021/acssuschemeng.9b07678
ACS Sustainable Chem. Eng. 2020, 8, 5903−5919

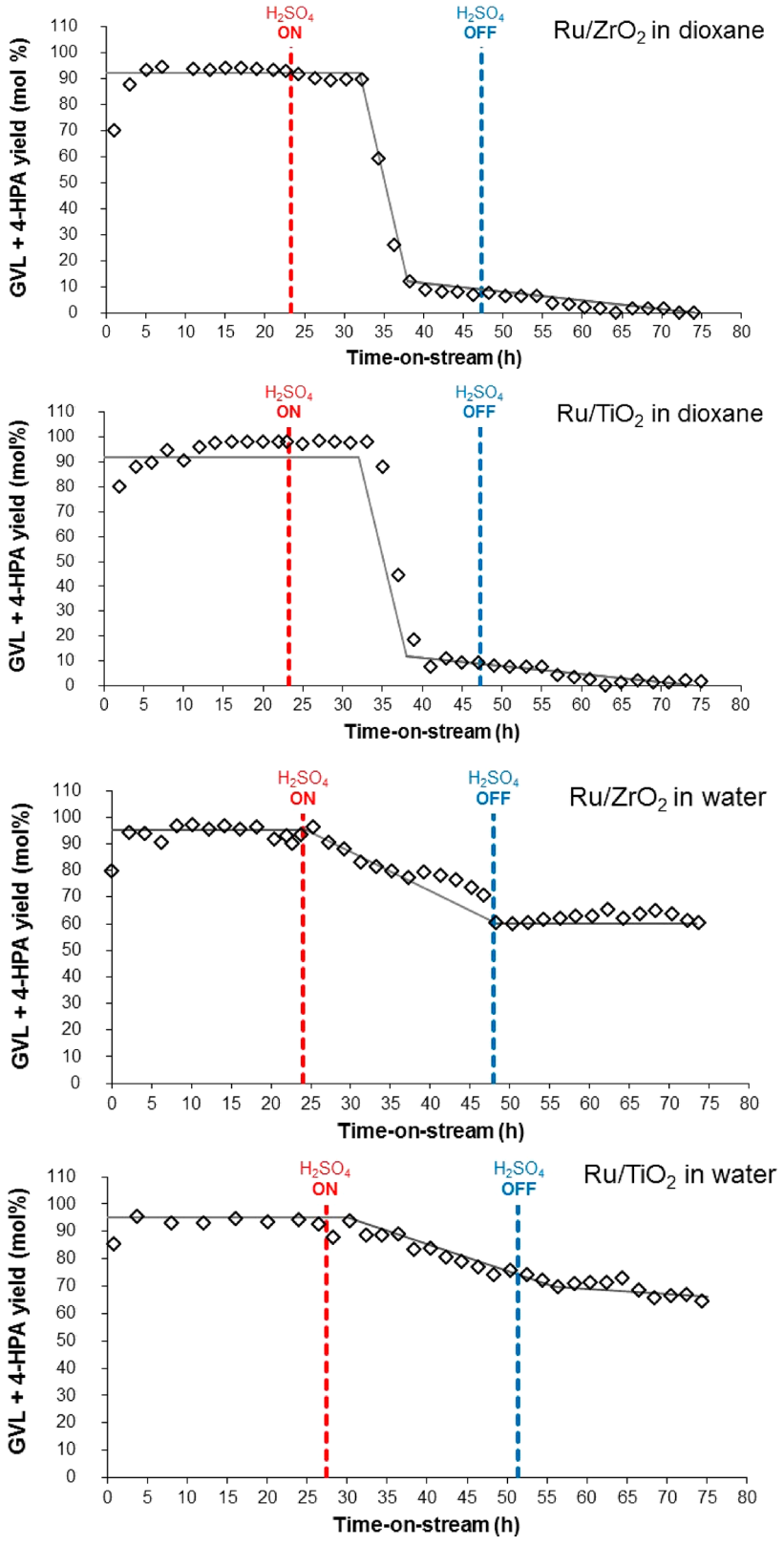

Figure 9. Influence of sulfuric acid on LA hydrogenation activity. Combined GVL and 4-HPA yields are given as a function of time-on-stream in a continuous-flow setup using 1 wt % Ru/ZrO_2 and 1 wt % Ru/TiO_2 catalysts in dioxane (150 °C) and water (90 °C).

50 h on-stream, the activity is regained, suggesting that FFR inhibits LA hydrogenation reversibly.

Previously, the inhibition of Ru catalysts by furanics such as HMF and FFR has been studied as part of a hydrodeoxygenation study for guaiacol in water at 270 °C.[32] It was found that the active sites of the Ru surface are preferentially occupied by FFR, thus suppressing guaiacol hydrogenation. In this present work, it is highly likely that the competitive

https://dx.doi.org/10.1021/acssuschemeng.9b07678
ACS Sustainable Chem. Eng. 2020, 8, 5903−5919

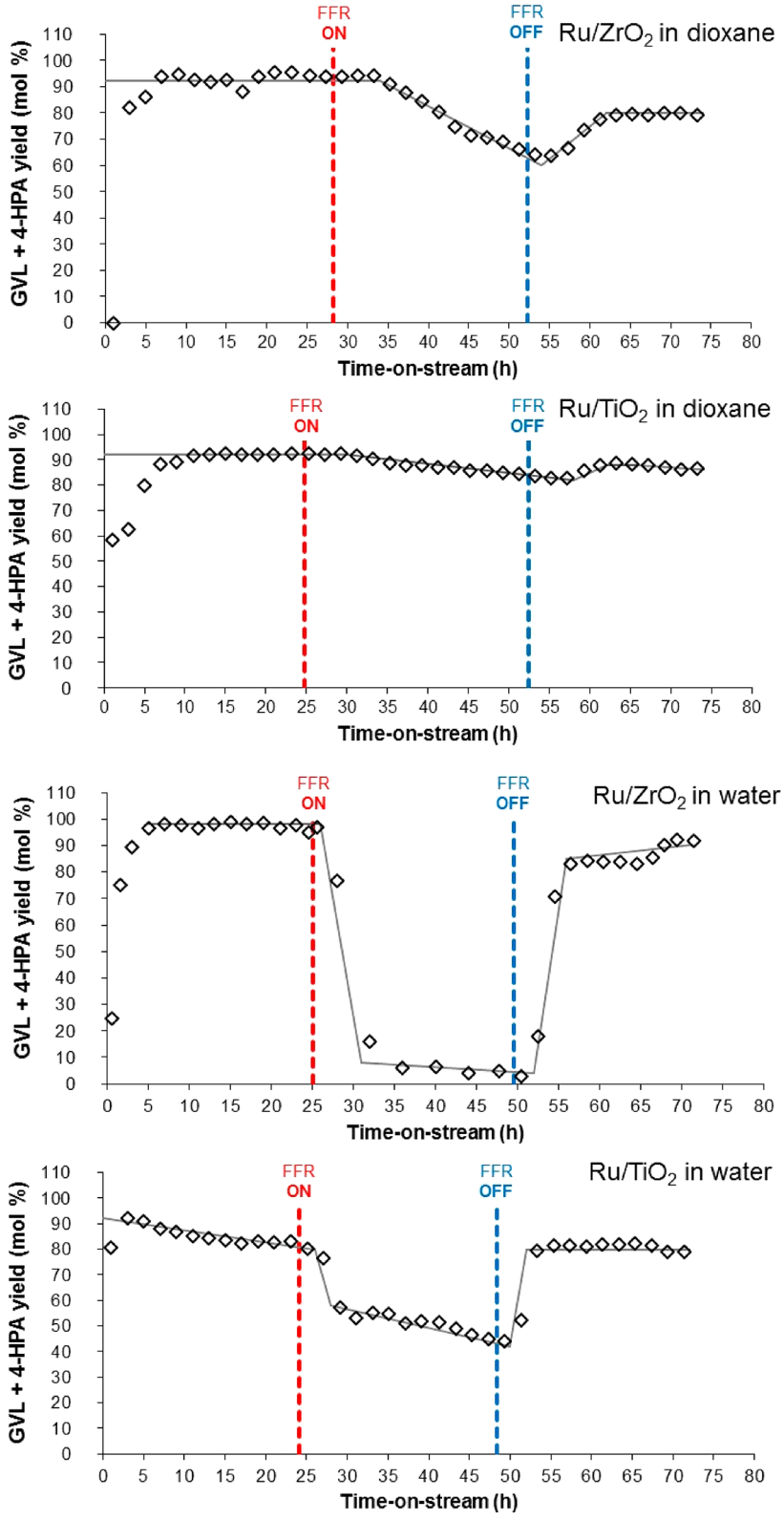

Figure 10. Influence of furfural on LA hydrogenation activity. Combined GVL and 4-HPA yields are given as a function of time-on-stream in a continuous-flow setup using 1 wt % Ru/ZrO_2 and 1 wt % Ru/TiO_2 catalysts in dioxane (150 °C) and water (90 °C).

adsorption of FFR on the catalyst surface results in catalyst inhibition. Catalyst fouling, e.g., by the deposition of larger organic fragments, is less likely (due to a lower temperature used), as this is expected to lead to irreversible deactivation. The latter is supported by TGA analysis of the spent catalysts, which shows low amounts of carbonaceous material after the reaction (3%). Furthermore, no significant changes in the textural properties were observed for the spent catalysts with and without FFR (Table 5). However, it cannot be excluded that FFR hydrogenation products, which are also inevitably

https://dx.doi.org/10.1021/acssuschemeng.9b07678
ACS Sustainable Chem. Eng. 2020, 8, 5903−5919

formed under the prevailing reaction conditions, also play a role. This was confirmed by the analogous batch experiments (Figure S10), which showed a number of hydrogenation products like furfuryl alcohol (major), 2-methylfuran, and tetrahydro-2-furanmethanol (GC-MS). The reversibility of catalyst inhibition by FFR is furthermore confirmed in batch recycle experiments in dioxane using Ru/ZrO_2 (Figure S11). Here, an increase in GVL yield was observed after the first reuse of the fresh catalyst, suggesting that some *in situ* activation of the catalyst also occurs. Stable performance was then observed upon recycling.

In water, the influence of FFR on the GVL yield is more pronounced for both catalysts than the influence found in dioxane. For instance, for Ru/ZrO_2, the GVL yield drops to below 5 mol % upon FFR addition. When switching back to the pure LA feed, the GVL yields increase dramatically, suggesting that catalyst inhibition by FFR is again reversible, as also found for dioxane.

The effect of the presence of HMF on LA hydrogenation activity was determined by batch experiments using Ru/ZrO_2 with a range of LA-to-HMF molar ratios. The GVL yield–time profiles for dioxane are given in Figure 11; additional

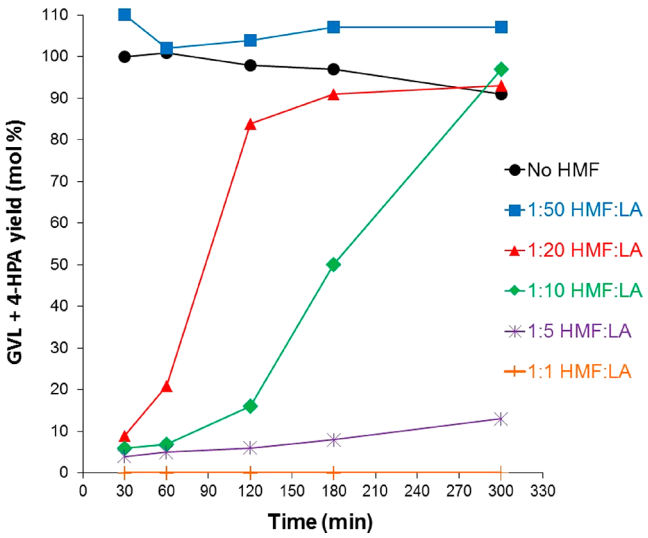

Figure 11. Influence of 5-hydroxymethylfurfural on LA hydrogenation activity. Combined GVL and 4-HPA yields are given as a function of time in a batch setup using 1 wt % Ru/ZrO_2 in dioxane in the presence of 5-hydroxymethylfurfural at different mole ratios with LA. Conditions: LA/Ru wt ratio of 400, 150 °C, and 50 bar H_2.

data for water are provided in the Supporting Information (see Figures S12, S13, and S14). The profiles are a strong function of the HMF/LA molar ratio, and no LA hydrogenation activity was observed at high HMF intakes at the start of a batch experiment. Upon lowering the HMF amount at the start of a batch reaction, LA hydrogenation occurs to a considerable extent. A run with a low (1:50) HMF/LA ratio gives a profile close to that observed for runs with LA only. At this low HMF concentration, mass balance closures greater than 100% were obtained, likely due to a subsequent reaction of HMF to LA, which is subsequently converted to GVL. A possible explanation for the effect of HMF on catalyst performance is the inhibition of the LA hydrogenation reaction due to the preferential adsorption of HMF to the active sites, as also found for FFR.

The influence of humins, invariably formed during the acid-catalyzed (hydrothermal) conversions of the carbohydrate fractions of lignocellulosic biomass,[33,34] on the performance of the Ru/TiO_2 catalyst for LA hydrogenation in water was investigated in a batch setup. A crude humin sample (liquid form, from Avantium; a byproduct of the conversion of C6 sugars to HMF in methanol as a solvent) was tested, which was previously found to contain 6.6 wt % carbonyl functions and is thought to be furan-rich.[33] The addition of 1 wt % crude humin sample (relative to the total weight of the mixture) had a major effect on the GVL yield versus time profile (Figure 12). These effects could be due to the presence of oligomeric humins but also due to low molecular weight impurities (HMF, HCOOH, etc.) present in the crude humins. An analysis of the reaction mixtures indeed confirmed the presence of hydrogenation products of HMF and methoxymethylfurfural. As such, it is difficult to draw conclusions regarding the influence of oligomeric humins on the Ru-catalyzed LA hydrogenation reaction. To reduce the complexity, additional experiments with purified humins obtained in a powder form were performed at 0.5 and 1 wt % intakes. A minor effect on catalyst performance was observed, likely due to the low solubility of the purified humins. Reactions in dioxane at 150 °C with the presence of 0.5 wt % purified humins gave a much stronger effect, likely due to the enhanced solubility of the humins in dioxane as compared to water.

Influence of Sulfur-Containing Amino Acids: Cysteine and Methionine. Batch LA hydrogenation experiments were performed with the Ru/ZrO_2 catalyst in dioxane in the presence of variable intakes of thiol- and thioether-containing amino acids (i.e., cysteine and methionine, respectively). Figure 13 shows that already at low loadings (e.g., 1:100 and 1:500 amino acid/LA mole ratios), a very strong inhibitory effect on the activity of Ru/ZrO_2 was detected. In contrast, nonsulfur-containing amino acids such as alanine did not have a major effect on the hydrogenation of LA to GVL. Deactivation was even more pronounced in water, as the Ru/TiO_2 catalyst lost activity even at trace levels of cysteine, with no GVL being detected after 300 min of reaction at 1:200 and 1:500 cysteine/LA mole ratios (Figure S15).

Recycling of the spent catalyst sample by a simple acetone wash did not restore the activity, as subsequent reuse with pure LA did not give any GVL yield. Leaching of Ru was found to be insignificant (ICP), and structural support changes were not observed. Thus, deactivation is likely to happen by an irreversible interaction of the sulfur-species with Ru and is considered permanent. Therefore, the effective removal of any biogenic sulfur-containing amino acid impurities from the LA feed is essential before the LA hydrogenation step.

CONCLUSIONS

Levulinic acid (LA) is a renewable platform chemical from which a large number of interesting biobased chemicals may be derived, including γ-valerolactone (GVL). Heterogeneous Ru-based catalysts are known to be particularly efficient for the hydrogenation of LA to GVL. However, insights in catalyst performance when using real feeds and the impurities expected therein are still limited but are highly relevant for the development of actual, efficient biorefinery processes involving LA and GVL synthesis. In this work, the stability of Ru/ZrO_2

https://dx.doi.org/10.1021/acssuschemeng.9b07678
ACS Sustainable Chem. Eng. 2020, 8, 5903–5919

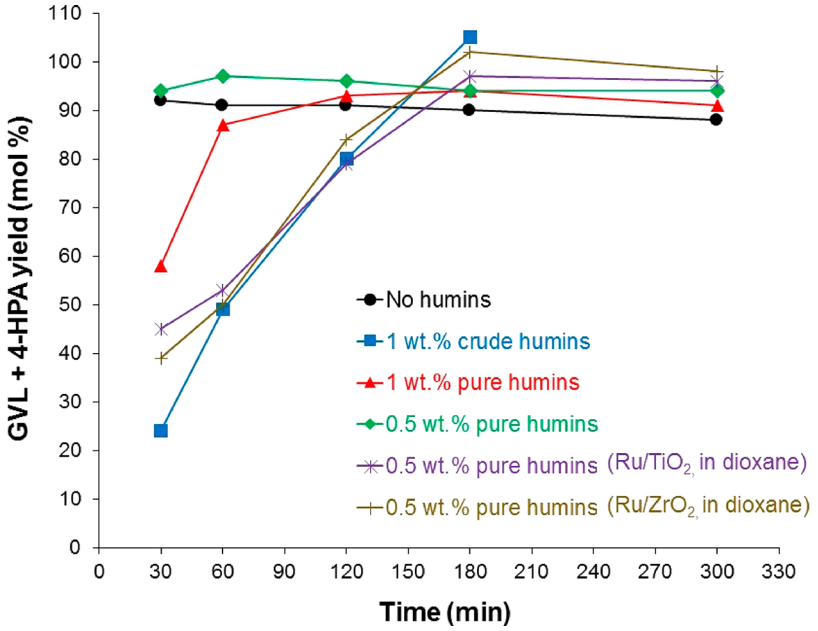

Figure 12. Influence of humins on LA hydrogenation activity. Combined GVL and 4-HPA yields are given as a function of time in a batch setup using 1 wt % Ru/TiO_2 catalyst in water in the presence of crude and purified industrial humins at different wt % intakes. Runs in dioxane using both catalysts are also presented for comparison. Conditions: LA/Ru wt ratio of 400, 90 °C (water), 150 °C (dioxane), and 50 bar H_2.

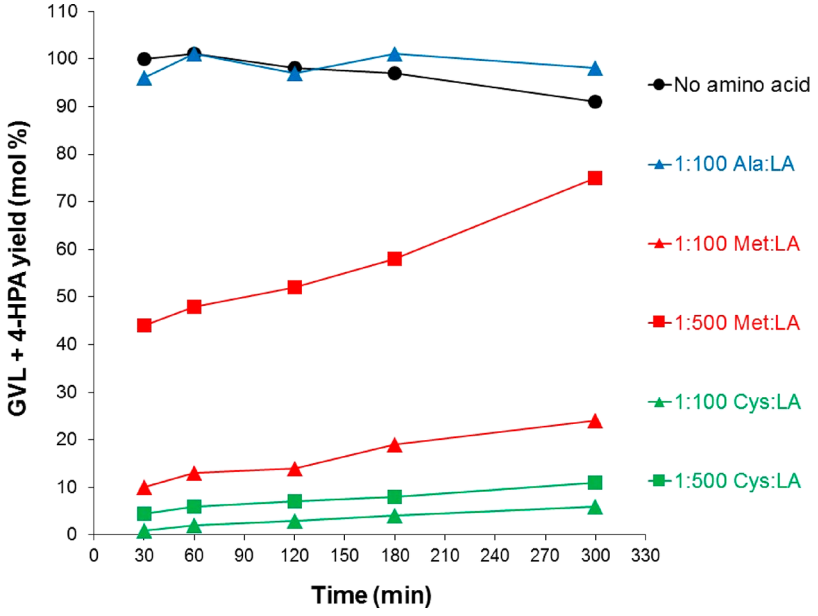

Figure 13. Influence of alanine, methionine, and cysteine on LA hydrogenation activity. Combined GVL and 4-HPA yields are given as a function of time in a batch setup using 1 wt % Ru/ZrO_2 catalyst in dioxane in the presence of amino acids at different mole ratios. Conditions: LA/Ru of 400, 150 °C, 50 bar H_2. Runs at 1:20 amino acid/LA mole ratio are given in Figure S16.

(monoclinic) and Ru/TiO_2 (P25) catalysts for LA hydrogenation in dioxane (a GVL mimic) and water was assessed in detail using continuous-flow experiments at long times on-stream. In addition, the influence of impurities on the stability of the Ru-based catalysts was studied in batch and continuous-flow units. Benchmark continuous-flow experiments using reagent-grade LA in dioxane showed that the Ru/ZrO_2 catalyst is more stable than the Ru/TiO_2 catalyst, whereas the reverse trend, though less pronounced, was observed in water. The characterization of the spent catalysts showed that the deactivation of Ru/TiO_2 in dioxane is mainly due to reduction of the TiO_2 support (XPS) and not by fouling (TGA) or Ru nanoparticle sintering (TEM). In water, deactivation is less severe for both catalysts and is likely caused by a combination of small effects. The addition of HCOOH proved detrimental for the LA hydrogenation reaction, giving almost complete, while reversible, inhibition of the catalysts. Catalytic inhibition by furfural and 5-hydroxymethylfurfural was also shown to be reversible and was likely due to the competitive adsorption of these furanics and/or their hydrogenation byproducts on the Ru surface. On the other hand, sulfur-containing components, such as H_2SO_4 and the amino acids cysteine and methionine, were found to lead to irreversible catalyst deactivation. These insights serve

https://dx.doi.org/10.1021/acssuschemeng.9b07678
ACS Sustainable Chem. Eng. 2020, 8, 5903−5919

as important input for the design of LA hydrogenation processes using Ru-based catalysts. Furthermore, this work not only guides future catalyst design but also provides relevant information for the separation and purification choices that need to be made in the downstream processing of LA.

■ ASSOCIATED CONTENT

Supporting Information

The Supporting Information is available free of charge at https://pubs.acs.org/doi/10.1021/acssuschemeng.9b07678.

XPS O 1s spectra and TEM images of fresh and spent Ru/ZrO_2 and Ru/TiO_2 catalysts and results of additional catalytic hydrogenation experiments in the batch setup (PDF)

■ AUTHOR INFORMATION

Corresponding Authors

Bert M. Weckhuysen − *Inorganic Chemistry and Catalysis, Debye Institute for Nanomaterials Science, Utrecht University, 3584 CG Utrecht, The Netherlands;* orcid.org/0000-0001-5245-1426; Email: b.m.weckhuysen@uu.nl

Pieter C. A. Bruijnincx − *Inorganic Chemistry and Catalysis, Debye Institute for Nanomaterials Science and Organic Chemistry and Catalysis, Debye Institute for Nanomaterials Science, Utrecht University, 3584 CG Utrecht, The Netherlands;* orcid.org/0000-0001-8134-0530; Email: p.c.a.bruijnincx@uu.nl

Hero J. Heeres − *Engineering and Technology Institute Groningen (ENTEG), Department of Chemical Engineering, University of Groningen, 9747 AG Groningen, The Netherlands;* orcid.org/0000-0002-1249-543X; Email: h.j.heeres@rug.nl

Authors

Homer C. Genuino − *Engineering and Technology Institute Groningen (ENTEG), Department of Chemical Engineering, University of Groningen, 9747 AG Groningen, The Netherlands; Inorganic Chemistry and Catalysis, Debye Institute for Nanomaterials Science, Utrecht University, 3584 CG Utrecht, The Netherlands*

Henk H. van de Bovenkamp − *Engineering and Technology Institute Groningen (ENTEG), Department of Chemical Engineering, University of Groningen, 9747 AG Groningen, The Netherlands*

Erwin Wilbers − *Engineering and Technology Institute Groningen (ENTEG), Department of Chemical Engineering, University of Groningen, 9747 AG Groningen, The Netherlands*

Jozef G. M. Winkelman − *Engineering and Technology Institute Groningen (ENTEG), Department of Chemical Engineering, University of Groningen, 9747 AG Groningen, The Netherlands;* orcid.org/0000-0001-7888-1731

Andrey Goryachev − *Laboratory for Inorganic Materials and Catalysis, Department of Chemical Engineering and Chemistry, Eindhoven University of Technology, 5600 MB Eindhoven, The Netherlands*

Jan P. Hofmann − *Laboratory for Inorganic Materials and Catalysis, Department of Chemical Engineering and Chemistry, Eindhoven University of Technology, 5600 MB Eindhoven, The Netherlands;* orcid.org/0000-0002-5765-1096

Emiel J. M. Hensen − *Laboratory for Inorganic Materials and Catalysis, Department of Chemical Engineering and Chemistry, Eindhoven University of Technology, 5600 MB Eindhoven, The Netherlands;* orcid.org/0000-0002-9754-2417

Complete contact information is available at: https://pubs.acs.org/10.1021/acssuschemeng.9b07678

Author Contributions

The manuscript was written through contributions of all authors. All authors have given approval to the final version of the manuscript.

Notes

The authors declare no competing financial interest.

■ ACKNOWLEDGMENTS

The authors gratefully acknowledge the Smart Mix Program of The Netherlands Ministry of Economic Affairs and The Netherlands Ministry of Education, Culture and Science within the framework of the Dutch CatchBio Program. The authors also thank Avantium Chemicals B.V. (The Netherlands) for providing the industrial humins samples. Dr. Fang Liu and Xiaoying Xi are acknowledged for their experimental support.

■ REFERENCES

(1) Lange, J.-P.; Price, R.; Ayoub, P.; Louis, J.; Petrus, L.; Clarke, L.; Gosselink, H. Valeric biofuels: a platform of cellulosic transportation fuels. *Angew. Chem., Int. Ed.* **2010**, *49*, 4479−4483.

(2) Wright, W. R. H.; Palkovits, R. Development of heterogeneous catalysts for the conversion of levulinic acid to γ-valerolactone. *ChemSusChem* **2012**, *5*, 1657−1667.

(3) Alonso, D. M.; Wettstein, S. G.; Dumesic, J. A. Gamma-valerolactone, a sustainable platform molecule derived from lignocellulosic biomass. *Green Chem.* **2013**, *15*, 584−595.

(4) Pileidis, F. D.; Titirici, M.-M. Levulinic acid biorefineries: New challenges for efficient utilization of biomass. *ChemSusChem* **2016**, *9*, 562−582.

(5) Zhang, Z. Synthesis of γ-valerolactone from carbohydrates and its applications. *ChemSusChem* **2016**, *9*, 156−171.

(6) Bond, J. Q.; Alonso, D. M.; Wang, D.; West, R. M.; Dumesic, J. A. Integrated catalytic conversion of gamma-valerolactone to liquid alkenes for transportation fuels. *Science* **2010**, *327*, 1110−1114.

(7) Fegyverneki, D.; Orha, L.; Láng, G.; Horváth, I. T. Gamma-valerolactone-based solvents. *Tetrahedron* **2010**, *66*, 1078−1081.

(8) Manzer, L. E. Catalytic synthesis of α-methylene-γ-valerolactone: A biomass-derived acrylic monomer. *Appl. Catal., A* **2004**, *272*, 249−256.

(9) Hengst, K.; Ligthart, D. A. J. M.; Doronkin, D. E.; Walter, K. M.; Kleist, W.; Hensen, E. J. M.; Grunwaldt, J.-D. Continuous synthesis of γ-valerolactone in a trickle-bed reactor over supported nickel catalysts. *Ind. Eng. Chem. Res.* **2017**, *56*, 2680−2689.

(10) Luo, W.; Sankar, M.; Beale, A. M.; He, Q.; Kiely, C. J.; Bruijnincx, P. C. A.; Weckhuysen, B. M. High performing and stable supported nano-alloys for the catalytic hydrogenation of levulinic acid to γ-valerolactone. *Nat. Commun.* **2015**, *6*, 6540−6550.

(11) Abdelrahman, O. A.; Luo, H. Y.; Heyden, A.; Román-Leshkov, Y.; Bond, J. Q. Toward rational design of stable, supported metal catalysts for aqueous-phase processing: Insights from the hydrogenation of levulinic acid. *J. Catal.* **2015**, *329*, 10−21.

(12) Liguori, F.; Moreno-Marrodan, C.; Barbaro, P. Environmentally friendly synthesis of γ-valerolactone by direct catalytic conversion of renewable sources. *ACS Catal.* **2015**, *5*, 1882−1894.

(13) Lange, J.-P. Renewable feedstocks: The problem of catalyst deactivation and its mitigation. *Angew. Chem., Int. Ed.* **2015**, *54*, 13186−13197.

(14) Luo, W.; Deka, U.; Beale, A. M.; Van Eck, E. R. H.; Bruijnincx, P. C. A.; Weckhuysen, B. M. Ruthenium-catalyzed hydrogenation of

levulinic acid: Influence of the support and solvent on catalyst selectivity and stability. *J. Catal.* **2013**, *301*, 175−186.
(15) Liu, F.; Ftouni, J.; Bruijnincx, P. C. A.; Weckhuysen, B. M. Phase-dependent stability and substrate-induced deactivation by strong metal-support interaction of Ru/TiO_2 catalysts for the hydrogenation of levulinic acid. *ChemCatChem* **2019**, *11*, 2079−2088.
(16) Ftouni, J.; Muñoz-Murillo, A.; Goryachev, A.; Hofmann, J.-P.; Hensen, E. J. M.; Lu, L.; Kiely, C. J.; Bruijnincx, P. C. A.; Weckhuysen, B. M. ZrO_2 is preferred over TiO_2 as support for the Ru-catalyzed hydrogenation of levulinic acid to γ-valerolactone. *ACS Catal.* **2016**, *6*, 5462−5472.
(17) Michel, C.; Zaffran, J.; Ruppert, A. M.; Matras-Michalska, J.; Jędrzejczyk, M.; Grams, J.; Sautet, P. Role of water in metal catalyst performance for ketone hydrogenation: A joint experimental and theoretical study on levulinic acid conversion into gamma-valerolactone. *Chem. Commun.* **2014**, *50*, 12450−12453.
(18) Michel, C.; Gallezot, P. Why is ruthenium an efficient catalyst for the aqueous-phase hydrogenation of biosourced carbonyl compounds? *ACS Catal.* **2015**, *5*, 4130−4132.
(19) Piskun, A. S.; Winkelman, J. G. M.; Tang, Z.; Heeres, H. J. Support screening studies on the hydrogenation of levulinic acid to γ-valerolactone in water using Ru catalysts. *Catalysts* **2016**, *6*, 131−151.
(20) Piskun, A. S.; Ftouni, J.; Tang, Z.; Weckhuysen, B. M.; Bruijnincx, P. C. A.; Heeres, H. J. Hydrogenation of levulinic acid to γ-valerolactone over anatase-supported Ru catalysts: Effect of catalyst synthesis protocols on activity. *Appl. Catal., A* **2018**, *549*, 197−206.
(21) Piskun, A. S.; de Haan, J. E.; Wilbers, E.; van de Bovenkamp, H. H.; Tang, Z.; Heeres, H. J. Hydrogenation of levulinic acid to γ-valerolactone in water using millimeter sized supported Ru catalysts in a packed bed reactor. *ACS Sustainable Chem. Eng.* **2016**, *4*, 2939−2950.
(22) Piskun, A. S.; van de Bovenkamp, H. H.; Rasrendra, C. B.; Winkelman, J. G. M.; Heeres, H. J. Kinetic modeling of levulinic acid hydrogenation to gamma-valerolactone in water using a carbon supported Ru catalyst. *Appl. Catal., A* **2016**, *525*, 158−167.
(23) Tan, J.; Cui, J.; Deng, T.; Cui, X.; Ding, G.; Zhu, Y.; Li, Y. Water-promoted hydrogenation of levulinic acid to γ-valerolactone on supported ruthenium catalyst. *ChemCatChem* **2015**, *7*, 508−512.
(24) Arena, B. Deactivation of ruthenium catalysts in continuous glucose hydrogenation. *Appl. Catal., A* **1992**, *87*, 219−229.
(25) Elliott, D. C.; Peterson, K. L.; Muzatko, D. S.; Alderson, E. V.; Hart, T. R.; Neuenschwander, G. G. Effects of trace contaminants on catalytic processing of biomass-derived feedstocks. *Appl. Biochem. Biotechnol.* **2004**, *115*, 807−826.
(26) Zhang, Z.; Jackson, J. E.; Miller, D. J. Effect of biogenic fermentation impurities on lactic acid hydrogenation to propylene glycol. *Bioresour. Technol.* **2008**, *99*, 5873−5880.
(27) Alamillo, R.; Crisci, A. J.; Gallo, J. M. R.; Scott, S. L.; Dumesic, J. A. A tailored microenvironment for catalytic biomass conversion in inorganic-organic nanoreactors. *Angew. Chem., Int. Ed.* **2013**, *52*, 10349−10351.
(28) Schwartz, T. J.; Johnson, R. L.; Cardenas, J.; Okerlund, A.; Da Silva, N. A.; Schmidt-Rohr, K.; Dumesic, J. A. Engineering catalyst microenvironments for metal-catalyzed hydrogenation of biologically derived platform chemicals. *Angew. Chem., Int. Ed.* **2014**, *53*, 12718−12722.
(29) Wang, H.; Lee, S.-J.; Olarte, M. V.; Zacher, A. H. Bio-oil stabilization by hydrogenation over reduced metal catalysts at low temperatures. *ACS Sustainable Chem. Eng.* **2016**, *4*, 5533−5545.
(30) Braden, D. J.; Henao, A. A.; Heltzel, J.; Maravelias, C. C.; Dumesic, J. A. Production of liquid hydrocarbon fuels by catalytic conversion of biomass-derived levulinic acid. *Green Chem.* **2011**, *13*, 1755−1765.
(31) Ftouni, J.; Genuino, H. C.; Muñoz-Murillo, A.; Bruijnincx, P. C. A.; Weckhuysen, B. M. Influence of sulfuric acid on the performance of ruthenium-based catalysts in the liquid-phase hydrogenation of levulinic acid to γ-valerolactone. *ChemSusChem* **2017**, *10*, 2891−2896.
(32) Dwiatmoko, A. A.; Lee, S.; Ham, H. C.; Choi, J.-W.; Suh, D. J.; Ha, J.-M. Effects of carbohydrates on the hydrodeoxygenation of lignin-derived phenolic compounds. *ACS Catal.* **2015**, *5*, 433−437.
(33) Constant, S.; Lancefield, C. S.; Weckhuysen, B. M.; Bruijnincx, P. C. A. Quantification and classification of carbonyls in industrial humins and lignins by ^{19}F NMR. *ACS Sustainable Chem. Eng.* **2017**, *5*, 965−972.
(34) Van Zandvoort, I.; Wang, Y.; Rasrendra, C. B.; van Eck, E. R.H.; Bruijnincx, P. C. A.; Heeres, H. J.; Weckhuysen, B. M. Formation, molecular structure, and morphology of humins in biomass conversion: Influence of feedstocks and processing conditions. *ChemSusChem* **2013**, *6*, 1745−1748.
(35) Naumkin, A.; Kraut-Vass, A.; Gaarenstroom, S. W.; Powell, C. J. *NIST X-ray Photoelectron Spectroscopy Database*. www.srdata.nist.gov/xps/ (accessed October 2019).
(36) Lin, T.; Yang, C.; Wang, Z.; Yin, H.; Lü, X.; Huang, F.; Lin, J.; Xie, X.; Jiang, M. Effective nonmetal incorporation in black titania with enhanced solar energy utilization. *Energy Environ. Sci.* **2014**, *7*, 967−972.
(37) Barreca, D.; Battiston, G. A.; Gerbasi, R.; Tondello, E.; Zanella, P. Zirconium dioxide thin films characterized by XPS. *Surf. Sci. Spectra* **2000**, *7*, 303−309.
(38) Umeda, K.; Miyasako, T.; Sugiyama, A.; Tanaka, A.; Suzuki, M.; Tokumitsu, E.; Shimoda, T. Impact of UV/O_3 treatment on solution-processed amorphous $InGaZnO_4$ thin-film transistors. *J. Appl. Phys.* **2013**, *113*, 184509−184514.
(39) Froment, G. F. Modeling of catalyst deactivation. *Appl. Catal., A* **2001**, *212*, 117−128.
(40) Fogler, H. S. Chapter 10: Catalysis and Catalytic Reactors. In *Elements of Chemical Reaction Engineering*, 5th ed.; Prentice Hall: Indiana, US, 2016; pp 454−456.
(41) Zhang, S.; Metin, Ö.; Su, D.; Sun, S. Monodisperse AgPd alloy nanoparticles and their superior catalysis for the dehydrogenation of formic acid. *Angew. Chem., Int. Ed.* **2013**, *52*, 3681−3684.
(42) Ruppert, A. M.; Jędrzejczyk, M.; Sneka-Płatek, O.; Keller, N.; Dumon, A. S.; Michel, C.; Sautet, P.; Grams, J. Ru catalysts for levulinic acid hydrogenation with formic acid as a hydrogen source. *Green Chem.* **2016**, *18*, 2014−2028.
(43) Al-Naji, M.; Popova, M.; Chen, Z.; Wilde, N.; Gläser, R. Aqueous-phase hydrogenation of levulinic acid using formic acid as a sustainable reducing agent over Pt catalysts supported on mesoporous zirconia. *ACS Sustainable Chem. Eng.* **2020**, *8*, 393−402.
(44) Al-Naji, M.; Van Aelst, J.; Liao, Y.; d'Hullian, M.; Tian, Z.; Wang, C.; Gläser, R.; Sels, B. Pentanoic acid from γ-valerolactone and formic acid using bifunctional catalysis. *Green Chem.* **2020**, *22*, 1171−1181.
(45) Yi, N.; Saltsburg, H.; Flytzani-Stephanopoulos, M. Hydrogen production by dehydrogenation of formic acid on atomically dispersed gold on ceria. *ChemSusChem* **2013**, *6*, 816−819.
(46) Ciftci, A.; Ligthart, D. A. J. M.; Pastorino, P.; Hensen, E. J. M. Nanostructured ceria supported Pt and Au catalysts for the reactions of ethanol and formic acid. *Appl. Catal., B* **2013**, *130−131*, 325−335.
(47) Schwartz, T. J.; O'Neill, B. J.; Shanks, B. H.; Dumesic, J. A. Bridging the chemical and biological catalysis gap: Challenges and outlooks for producing sustainable chemicals. *ACS Catal.* **2014**, *4*, 2060−2069.
(48) König, C. F. J.; Schuh, P.; Huthwelker, T.; Smolentsev, G.; Schildhauer, T. J.; Nachtegaal, M. Influence of the support on sulfur poisoning and regeneration of Ru catalysts probed by sulfur K-edge X-ray absorption spectroscopy. *Catal. Today* **2014**, *229*, 56−63.

https://dx.doi.org/10.1021/acssuschemeng.9b07678
ACS Sustainable Chem. Eng. 2020, 8, 5903−5919